J Comput Neurosci (2015) 39:349–370
DOI 10.1007/s10827-015-0580-6

Information filtering in resonant neurons

Sven Blankenburg[1,2,3] · **Wei Wu**[4] · **Benjamin Lindner**[1,3] · **Susanne Schreiber**[1,2]

Received: 26 February 2015 / Revised: 23 September 2015 / Accepted: 29 September 2015 / Published online: 6 November 2015

Abstract Neuronal information transmission is frequency specific. In single cells, a band-pass like frequency preference can arise from the subthreshold dynamics of the membrane potential, shaped by properties of the cell's membrane and its ionic channels. In these cases, a cell is termed *resonant* and its membrane impedance spectrum exhibits a peak at non-vanishing frequencies. Here, we show that this frequency selectivity of neuronal response amplitudes need not translate into a similar frequency selectivity of information transfer. In particular, neurons with resonant but *linear* subthreshold voltage dynamics (without threshold) do not show a resonance of information transfer at the level of subthreshold voltage; the corresponding coherence has low-pass characteristics. Interestingly, we find that when combined with nonlinearities, subthreshold resonances do shape the frequency dependence of coherence and the peak in the subthreshold impedance translates to a peak in the coherence function. In other words, the nonlinearity inherent to spike generation allows a subthreshold *impedance* resonance to shape a resonance of voltage-based *information transfer*. We demonstrate such nonlinearity-mediated band-pass filtering of information at frequencies close to the subthreshold impedance resonance in three different model systems: the resonate-and-fire model, the conductance-based Morris-Lecar model, and linear resonant dynamics combined with a simple static nonlinearity. In the spiking neuron models, the band-pass filtering is most pronounced for low firing rates and a high variability of interspike intervals, similar to the spiking statistics observed in vivo. We show that band-pass filtering is achieved by reducing information transfer over low-frequency components and, consequently, comes along with an overall reduction of information rate. Our work highlights the crucial role of nonlinearities for the frequency dependence of neuronal information transmission.

Keywords Resonate-and-fire models · Information filtering · Frequency tuning · Coherence function · Static nonlinearity

Action Editor: Tim Gollisch

✉ Susanne Schreiber
s.schreiber@hu-berlin.de

[1] Bernstein Center for Computational Neuroscience Berlin, Berlin, Germany

[2] Institute for Theoretical Biology, Department of Biology, Humboldt-Universität zu Berlin, Berlin, Germany

[3] Department of Physics, Humboldt-Universität zu Berlin, Berlin, Germany

[4] Hefei National Laboratory for Physical Sciences at the Microscale, University of Science and Technology of China, Hefei, 230026 Anhui, China

1 Introduction

The transmission of time-dependent signals in the brain is frequency dependent. Zooming in on the subthreshold membrane-potential dynamics of single neurons, one often encounters low-pass filtering of signals, i.e. the responses to time-dependent inputs exhibit largest amplitudes for lower frequencies and attenuate for higher frequencies of the incoming signal. Alternatively, signal transfer can also show

band-pass characteristics, i.e. response amplitudes peak in a preferred range of frequencies and decline for lower as well as higher surrounding frequencies. The latter case is also termed "resonant". Such resonances have been well described for the intrinsic dynamics of subthreshold voltages in a number of different cell types (see, for example, Mauro et al. 1970; Alonso and Llinas 1989; Puil et al. 1994; Gutfreund et al. 1995; Gloveli et al. 1997; Engel et al. 2008) and have been described theoretically (see, for example, Hutcheon and Yarom 2000; Izhikevich 2001; Brunel et al. 2003; Engel et al. 2008; Rotstein and Nadim 2014).

In this study, we address the question to what extent a resonance in the subthreshold voltage amplitude also impacts the amount of *information* conveyed both in a neuron's graded, subthreshold voltage response as well as in its spikes. One might assume that larger amplitudes in a preferred frequency band due to subthreshold resonances result in a particularly high information transfer between input and response in this frequency band. This intuition, however, has not yet been explored at the single cell level and here we put it to the test by analyzing the frequency dependence of information transfer in neuronal systems exhibiting resonances of response amplitudes when stimulated with time-dependent input signals.

Specifically, we analyze a frequency-resolved measure of information transmission: the spectral coherence function. We show that the naive assumption that the amplitude resonance also shapes the frequency dependence of information transfer is not necessarily true. In particular, for linear systems (such as the pure subthreshold response of a resonator neuron), information transfer at resonant frequencies is not favored; the frequency dependence of information transfer always exhibits broadband characteristics despite resonances in response amplitude. Interestingly, however, our analysis also predicts that a neuron's nonlinearities are well suited to "pass on" resonances from amplitudes to the level of spike-based information transfer at the single cell level. A resonance in the subthreshold dynamics hence represents a mechanism for frequency-selective information transfer with spikes.

Other mechanisms for such information filters have previously been described, including short-term-plasticity (Lindner et al. 2009; Rosenbaum et al. 2012; Droste et al. 2013) or synchrony coding in neural populations (Middleton et al. 2009; Sharafi et al. 2013). In contrast to these mechanisms, the kind of information filtering considered here originates in the subthreshold dynamics of the single cell.

In this study, we analyze three conceptually different model systems in a neuronal context: a resonate-and-fire model, a classic conductance-based model (Morris-Lecar), and a simple linear-nonlinear (LN) model combining linear dynamics with a static nonlinearity. We find that while resonances in response amplitude do not translate to resonances in information characterized by the corresponding coherence, nonlinearities "transfer" a resonance to the level of the coherence in all three cases. Our results demonstrate that for neuronal systems, subthreshold resonances of the membrane potential indeed do shape a resonance in the spike-based information transfer in these neurons. The subthreshold dynamics (together with suitable nonlinearities) can create a frequency band where information transfer is favored. Altogether, the crucial role of nonlinearities in the frequency dependence of information transfer is likely to extend beyond the neuronal context to other biological signaling pathways that process time-dependent inputs.

2 Methods

2.1 Models of resonant neurons

Many neurons show resonant properties, which can be observed in experiments (see, for instance, Gutfreund et al. 1995; Hutcheon et al. 1996; Hu et al. 2002) and predicted in theoretical models (see Rinzel and Ermentrout 1989; Izhikevich 2001; Brunel et al. 2003; Erchova et al. 2004). While a resonance of the subthreshold membrane impedance leads to largest *amplitudes* of the membrane potential when stimulated in a specific frequency band, we here want to test the *information transfer*. As of now it has not been investigated to what extent the subthreshold resonant properties affect information transfer in either the subthreshold or the spiking regime. Different mathematical models are known to capture subthreshold resonance. These include two prominent, though conceptually different types: (1) the simpler resonate-and-fire models, which combine differential equations capturing the linear subthreshold dynamics with a static firing threshold and a voltage reset (Izhikevich 2001), and (2) conductance-based models including the nonlinear dynamics of spike initiation. To investigate information transmission, we here analyze the resonate-and-fire (RF) neuron (Izhikevich 2001) in the mathematical description by Engel et al. (2008), as well as the conductance-based Morris-Lecar (ML) model (Morris and Lecar 1981) in a simplified version by Rinzel and Ermentrout (1989). To support our finding that nonlinear properties of the neuronal dynamics play a crucial role for the frequency dependence of information transfer, we additionally investigate an artificial dynamical system: the purely linear subthreshold dynamics of the RF model when directly combined with a static nonlinearity. In the following, we introduce these models in more detail and begin with the isolated subthreshold dynamics of the RF model, i.e. without threshold and reset (and without static nonlinearity).

2.1.1 Linear, resonant dynamics of the subthreshold membrane potential (non-spiking model)

We first consider the following two-dimensional, linear neuron model that can display subthreshold resonance, but also low-pass filter characteristics of the impedance, depending on the choice of its parameters. We follow the formulation of Erchova et al. (2004) and Engel et al. (2008):

$$C\frac{d}{dt}V(t) = -\frac{1}{R}V(t) - I_L(t) + \xi(t) + s(t) + I_0, \quad (1)$$

$$L\frac{d}{dt}I_L(t) = -R_{\mathrm{L}}I_L(t) + V(t) - V_{\mathrm{rest}}\left(1 + \frac{R_{\mathrm{L}}}{R}\right). \quad (2)$$

Here, $V(t)$ is the membrane potential, I_L is a slow membrane current, C is the membrane capacitance, R and R_{L} are resistances, L is an inductance and V_{rest} the resting potential. Note that $V_0 = V_{\mathrm{rest}}(1 + R_{\mathrm{L}}/R)$ corresponds to battery term (see equivalent circuit in Fig. 1a). In the absence of noise the system approaches the fixed point

$$V_{\mathrm{FP}} = \frac{R_{\mathrm{L}}}{\left(\frac{R_{\mathrm{L}}}{R} + 1\right)}I_0 + V_{\mathrm{rest}}, \quad (3)$$

$$I_{\mathrm{FP}} = \frac{1}{\left(\frac{R_{\mathrm{L}}}{R} + 1\right)}I_0 - \frac{V_{\mathrm{rest}}}{R}, \quad (4)$$

which can be controlled for both variables by the constant input current I_0. The intrinsic current noise $\xi(t)$ is Gaussian white noise with intensity D and correlation $\langle\xi(t)\xi(t')\rangle = 2D\delta(t - t')$.

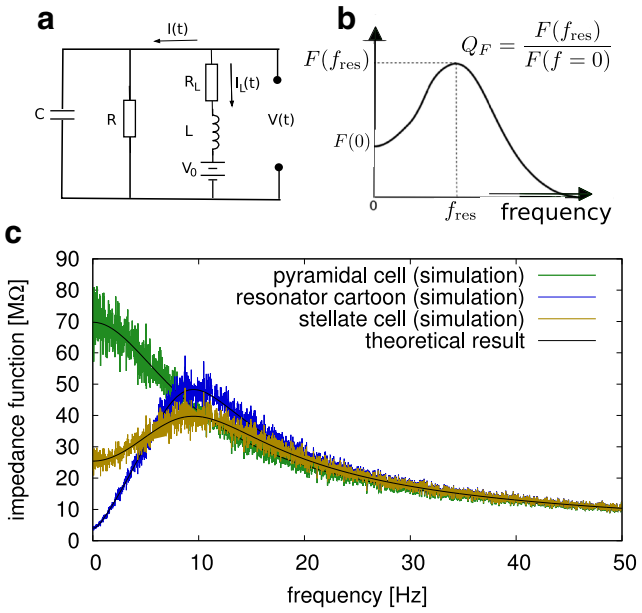

Fig. 1 Resonance in the linear, subthreshold dynamics (without threshold). **a** Equivalent circuit description. **b** Definition of the quality measure Q_F of a peaked spectral function. **c** Impedance functions for the three parameter sets (i)–(iii) chosen for illustration (resonator cartoon, stellate, and pyramidal cell)

To test for resonances, stimulation can be based on any time-dependent stimuli that exhibit power in the frequency range of interest. In experiments, it is common practice to use pure sine waves or sine waves whose frequency is modulated in time (such as ZAP stimuli, see, for example Gimbarzevsky et al. 1984). Alternatively, time-dependent noise stimuli can be used as well (yielding mathematically equivalent results in linear systems). We here adopt the latter approach and model and the external current signal $s(t)$ as an Ornstein-Uhlenbeck (OU) process

$$\tau_{\mathrm{OU}}\frac{d}{dt}s(t) = -s(t) + \xi_{\mathrm{OU}}(t), \quad (5)$$

with correlation time τ_{OU} and noise intensity D_{OU}. We choose an OU process in order to mimic low-pass filtered real-world stimuli (for instance, due to synaptic filtering processes), which are also routinely used in experimental studies (see for example Badel et al. 2008). The Gaussian noise $\xi_{\mathrm{OU}}(t)$ in Eq. (5) is uncorrelated in time (white) with $\langle\xi_{OU}(t)\xi_{\mathrm{OU}}(t')\rangle = 2D_{\mathrm{OU}}\delta(t - t')$ and independent of the intrinsic noise $\xi(t)$. The OUP $s(t)$ itself is a Gaussian noise that is exponentially correlated over time and possesses a Lorentzian power spectrum

$$S_{\mathrm{s,s}}(f) = \frac{2D_{\mathrm{OU}}}{1 + (2\pi f\tau_{\mathrm{ou}})^2}. \quad (6)$$

f denotes the frequency and is hence the independent variable of the power spectral density of the stimulus. According to Eq. (6), most power is located at low frequencies and there is no resonant peak.

To investigate the properties of information transfer we consider two derived characteristics of the model: the natural frequency f_{nat} and the damping factor ζ (which can be read off responses to brief stimulation with a puls, the so-called impulse response), defined as

$$f_{\mathrm{nat}} = \frac{\sqrt{\frac{4}{CL} - \left(\frac{1}{RC} - \frac{R_{\mathrm{L}}}{L}\right)^2}}{4\pi}, \zeta = \frac{\frac{1}{R} + \frac{R_{\mathrm{L}}C}{L}}{2\sqrt{\frac{C}{L}\left(1 + \frac{R_{\mathrm{L}}}{R}.\right)}}. \quad (7)$$

Resonance of the membrane impedance, i.e. a resonance in the amplitude of the subthreshold voltage response, is characterized by the complex-valued impedance function $Z(f)$, which for the subthreshold part of the RF model reads

$$Z(f) = \frac{(2\pi if)\,L + R_{\mathrm{L}}}{\left(\frac{R+R_{\mathrm{L}}}{R} - (2\pi f)^2\,LC\right) + (2\pi if)\left(\frac{L}{R} + R_{\mathrm{L}}C\right)}. \quad (8)$$

In the so-called underdamped parameter regime (defined by $\zeta < \frac{1}{\sqrt{2}}$), the impedance has a pronounced maximum at the resonance frequency

$$f_{\text{res}}^{\text{Z}} = \frac{1}{2\pi}\sqrt{\sqrt{\frac{1}{C^2L^2} + \frac{2R_{\text{L}}}{CL^2}\left(\frac{R_{\text{L}}}{L} + \frac{1}{RC}\right)} - \frac{R_{\text{L}}^2}{L^2}}, \quad (9)$$

which is in general different from the natural frequency f_{nat} in Eq. (7).

In order to quantify how pronounced a resonance is, we use the quality factor Q_Z. It is defined by the ratio between the value at the peak of the impedance function and the value at 0 Hz (see Fig. 1b) and can, in principle, be applied to any resonant spectral function $F(f)$

$$Q_{\text{F}} = \frac{|F(f_{\text{res}})|}{|F(f=0)|}. \quad (10)$$

Later on, we accordingly use the quality factor to quantify a resonant peak in our measure of information transmission, the spectral coherence. For the membrane impedance, $Q_{\text{Z}} \approx 1$ indicates that the system transmits most power at low frequencies (low-pass filter). In contrast, Q_{Z} significantly larger than one is a signature of band-pass filtering. For the subthreshold dynamics of the RF model, Q_{Z} reads

$$Q_{\text{Z}} = \sqrt{\frac{\left(1+\frac{R}{R_{\text{L}}}\right)}{1+2\left(\frac{CR^2}{L}\right)\left(\sqrt{1+2\frac{R_{\text{L}}}{R}+2\frac{CR_{\text{L}}^2}{L}} - \frac{R_{\text{L}}+2R}{2R}\right)}}, \quad (11)$$

and in the limit of large inductance L approaches

$$\lim_{L\to\infty} Q_{\text{Z}} = \sqrt{\left(1+\frac{R}{R_{\text{L}}}\right)}. \quad (12)$$

To explore information transmission in resonant neurons, we systematically varied many of the parameters governing the subthreshold dynamics described in this section (> 75.000 parameter sets, see results in Figs. 6, 8 and 9–11). For the clarity of presentation, we chose three specific parameter sets (see Table 1 and Fig. 1c) to illustrate our findings in more detail. These parameter sets correspond to (i) a model with exceedingly strong resonance (termed "resonator cartoon"), (ii) a model previously adapted to capture the experimentally measured impedance of resonant cells in the entorhinal cortex (termed "stellate cell"), and (iii) a non-resonant cell with parameters as previously characterized for nonresonant cells in the entorhinal cortex (termed "pyramidal cell"), see also Schreiber et al. (2004) for details on the last two cases.

Table 1 Three different parameter sets of the RF model used for illustration

Parameter	Resonator cartoon	Stellate cell (EC-II)	Pyramidal cell (EC-III)
$R\ [M\Omega]$	51.6	56.7	69.9
$R_{\text{L}}\ [M\Omega]$	4.4	46.1	34661.0
$L\ [MH]$	0.97	1.26	173.0
$C\ [pF]$	310	310	310
$V_{\text{thresh}}\ [mV]$	−59.2	−59.5	−60.5
$V_{\text{rest}}\ [mV]$	−63.5	−63.5	−63.5
$V_{\text{reset}}\ [mV]$	−75.0	−75.0	−75.0
$\tau_{\text{abs}}\ [ms]$	50	50	50
$I_0[nA]$	4.10	0.65	0.24
D $[10^{-6}(nA/s)^2]$	6.40	6.97	4.44
D_{OU} $[10^{-5}(nA/s)^2]$	5.18	5.53	2.60

For stellate and pyramidal cells, R, R_L, L, C adopted from Schreiber et al. (2004). Input and noise parameters are stated below the dashed line

2.1.2 Spiking resonate-and-fire neuron model

While Eqs. (1) and (2) in the previous section capture the purely subthreshold dynamics, a spiking model can be obtained by combination with a voltage threshold followed by a reset, which introduces a strong nonlinearity in the system. Two reset rules have previously been applied:

- if V reaches a threshold V_{thresh} then V is reset to $V_{\text{reset}} < V_{\text{thresh}}$ (I_{L} is not affected),
- if V reaches a threshold V_{thresh} then V and I_L are reset to $V_{\text{reset}} < V_{\text{thresh}}$ and $I_L = I_{\text{L,reset}}$.

The first reset rule (where I_L is not directly affected) is used in the generalized integrate-and-fire model (Brunel et al. 2003; Richardson et al. 2003). We follow Engel et al. (2008) and use the second rule, including an absolute refractory period τ_{abs}

$$V(t) \geq V_{\text{thresh}} \quad \Rightarrow \quad \begin{array}{l} V(t+\tau_{abs}) = V_{\text{reset}}, \\ I_L(t+\tau_{abs}) = I_0 - \frac{V_{\text{reset}}}{R} \end{array} . \quad (13)$$

Equation (13) implies that the derivative of the membrane voltage (of the deterministic system) at the reset value V_{reset} is zero. This is motivated by the fact that at the minimum of the hyperpolarization following a spike, the first derivative of the membrane potential with respect to time is always zero.

The described fire-and-reset rule generates a point process with an associated spike train $x(t)$, where $x(t) = \sum_i \delta(t-t_i)$, with spikes at time points t_i defined by the threshold crossing of the voltage variable. In Fig. 2a1, a2 the dynamics of the model are illustrated.

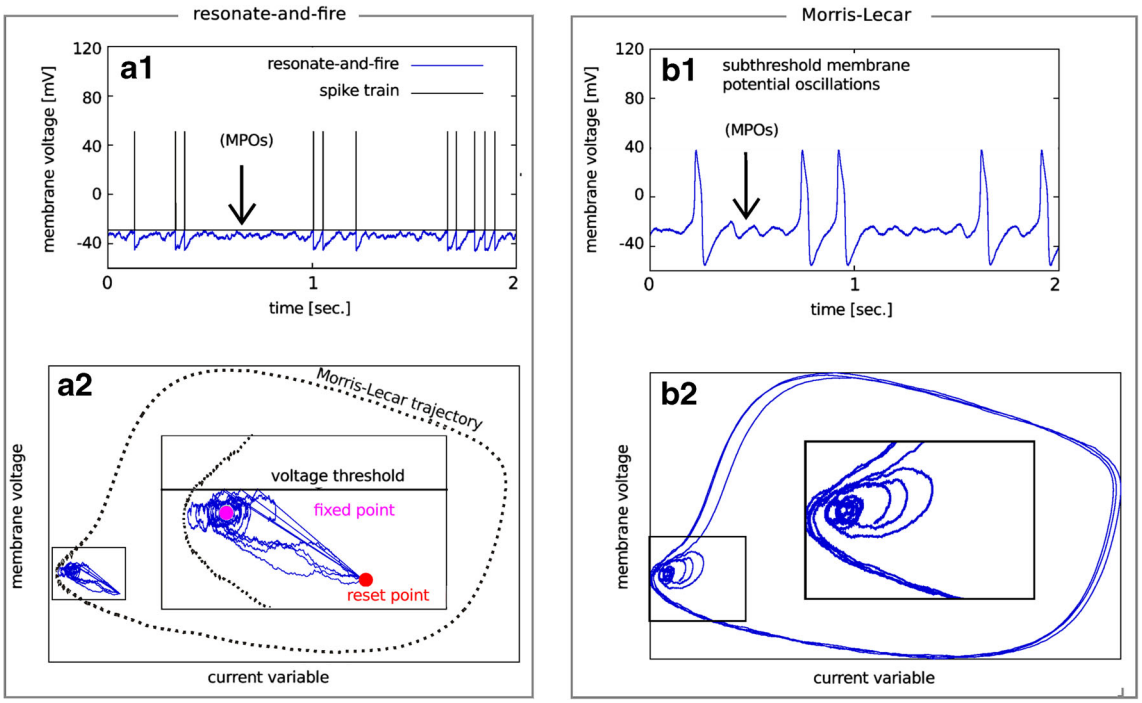

Fig. 2 Two models with subthreshold resonance. Membrane voltage trace and spike train for the RF model (**a1**), where spikes have been added by hand, as well as for the Morris-Lecar (ML) model (**b1**), capturing the full spike dynamics; see also expanded views in (**a2**) and (**b2**), respectively. ML phase-plane trajectory (*dotted line*) included in (**a2**) for comparison to the discontinuous phase portraits of the RF model (*blue line*). For model parameters see Table 1 ("resonator cartoon" without absolute refractory period) and Table 4 (ML, type II)

With respect to the fixed point (FP) Eq.(3) in the absence of a reset rule, three regimes can be distinguished:

- FP below threshold for $I_0 < (V_{\text{thresh}} - V_{\text{rest}})\left(\frac{1}{R_L} + \frac{1}{R}\right)$,
- FP close to threshold $I_0 \approx (V_{\text{thresh}} - V_{\text{rest}})\left(\frac{1}{R_L} + \frac{1}{R}\right)$,
- FP above threshold for $I_0 > (V_{\text{thresh}} - V_{\text{rest}})\left(\frac{1}{R_L} + \frac{1}{R}\right)$.

We note that even without noise and for a fixed point below threshold, the resonant (oscillatory) dynamics in conjunction with an appropriate reset condition leads to tonic firing. This is in marked contrast to the integrator (i.e. nonresonant) neurons in our study, for which a fixed point below threshold necessarily implies that the neuron generates a spike only by time-dependent input. This latter effect is ensured by the specific choice of our reset rule, Eq. (13), and does not generalize to other reset rules with $(dV/dt|_{V=V_{\text{reset}}} \neq 0)$.

2.1.3 Morris-Lecar model

In the RF model described above, spikes are obtained via an explicit threshold. We chose to also analyze the Morris-Lecar (ML) model (Morris and Lecar 1981) for its different spike-generating mechanism. Here, spikes arise directly from the nonlinear dynamics of the differential equations. Furthermore, the model can be tuned to display either type I or type II dynamics (Rinzel and Ermentrout 1989; Gutkin and Ermentrout 1998; Izhikevich 2007), with spike initiation via a saddle-node on an invariant cycle or a subcritical Hopf bifurcation, respectively. We here use two parameter sets, corresponding to type I and type II (see Table 4). As a consequence, the model is nonresonant (low-pass impedance) in the type I parameter set and resonant in the type II parameter set. We consider the ML model in a simplified two-dimensional version (Rinzel and Ermentrout 1989):

$$C\frac{dV}{dt} = -g_{\text{Ca}} m_\infty(V)\,(V - E_{\text{Ca}}) - g_{\text{K}} w\,(V - E_{\text{K}}) - \\ -g_L\,(V - E_{\text{L}}) + \eta(t) + s(t), \tag{14}$$

$$\frac{dw}{dt} = \Phi\frac{w_\infty(V) - w}{\tau_w(V)}, \tag{15}$$

where V is the membrane potential (fast variable) and w the potassium gating variable (slow recovery variable). The parameters $g_{\text{Ca}}, g_{\text{K}}, g_{\text{L}}$ and $E_{\text{Ca}}, E_{\text{K}}, E_{\text{L}}$ denote the peak conductances and the reversal potentials for calcium, potassium, and leak conductance, respectively. The activation functions for the voltage dependent Ca^{2+} and K^+ conduc-

tances as well as the time constant of the latter are given by

$$m_\infty(V) = 0.5\left(1+\tanh\left(\frac{V-V_1}{V_2}\right)\right), \quad (16)$$

$$w_\infty(V) = 0.5\left(1+\tanh\left(\frac{V-V_3}{V_4}\right)\right), \quad (17)$$

$$\tau_w(V) = \frac{1}{\cosh\left(\frac{V-V_3}{2V_4}\right)}. \quad (18)$$

A sample trajectory of the resonant (i.e. type II) model is displayed in Fig. 2a2, b2. As for the RF model, a voltage threshold of 0 mV is used to identify spike times t_i, mathematically defining the spike train $x(t) = \sum \delta(t - t_i)$.

2.2 Model with a static nonlinearity

To test a third type of nonlinearity, we consider the purely subthreshold dynamics of the RF model (Eqs. (1) and (2)) combined with a static nonlinearity F, acting on the voltage $V(t)$ (hence producing the continuous model output $F(V(t))$). Specifically, we use a sigmoidal nonlinearity based on the error function

$$F(V(t)) = \frac{\left(1+\mathrm{erf}\left(\frac{\gamma}{\sqrt{2}}(V(t)-\mu)\right)\right)}{2}, \quad (19)$$

where γ determines the maximal slope of the sigmoid. The constant offset μ sets the voltage of the inversion point of the sigmoid, where *F(V)* amounts to 50 % of the maximal value. For comparison, we also analyze a Heaviside step function $F(V) = \Theta(V(t) - \mu)$ centered around $V = \mu$, which corresponds to the limit $\gamma \to \infty$ in Eq. (19).

The degree of nonlinearity that values of V are actually subjected to in this simple model depends on the relative location of the distribution of V (here termed $P(V)$) with respect to the inversion point of the sigmoid as well as on the standard deviation of $P(V)$. As a measure of "effective nonlinearity" we introduce the quantity $\Gamma_{\mathrm{F(V)}}$ by

$$\Gamma_{\mathrm{F(V)}} = \int_{-\infty}^{+\infty} P(V)F'^2(\gamma;\mu,V)dV - \left(\int_{-\infty}^{+\infty} P(V)F'(\gamma;\mu,V)dV\right)^2. \quad (20)$$

This measure directly quantifies the variance of the distribution of slopes $(\partial F/\partial V)$ of the static nonlinearity that is actually sampled by the distribution of voltages $P(V)$. If the variance of this distribution of local slopes is very small, the transformation is nearly linear. In contrast, if the variance is very large, the transformation is strongly nonlinear. Especially, for any system with linear voltage dynamics, like the subthreshold voltage dynamics defined by Eqs. (1) and (2), the voltage distribution is Gaussian, $P(V) = e^{-\frac{V^2}{2\sigma^2}}/\sqrt{2\pi}\sigma$. For the error function as a static nonlinearity, Γ hence reads

$$\Gamma_{\mathrm{erf}} = \frac{(\gamma/\sigma)^2}{2\pi}\left(\frac{e^{-\frac{\gamma^2\mu^2}{1+2\gamma^2\mu^2}}\sigma}{2\gamma^2+\frac{1}{\sigma^2}} - \frac{e^{-\frac{\gamma^2\mu^2}{1+\gamma^2\mu^2}}}{\sqrt{\gamma^2+\frac{1}{\sigma^2}}}\right). \quad (21)$$

Γ_{erf} is illustrated in Fig. 3 for various combinations of slope factor γ and offset μ.

2.3 Spike train statistics and spectral measures of information transmission

To characterize responses and measure information transmission we introduce several relevant quantities.

Firing rate and coefficient of variation (CV) The sequence of interspike intervals (ISIs) $T_i = t_{i+1} - t_i$ is based on the measured spike times t_i. Firing rate and CV of the ISI are quantified as

$$r = \frac{1}{\langle T_i\rangle}, \quad \mathrm{CV} = \frac{\sqrt{\langle (T_i - \langle T_i\rangle)^2\rangle}}{\langle T_i\rangle}, \quad (22)$$

where $\langle\cdot\rangle$ represents an average over the interval sequence. A CV close to zero indicates a regular spike train, a purely random (Poisson) spike train entails a CV of one, whereas bursting is revealed by a CV that exceeds unity.

Spectral measures of variability and input-output correlations Let $y(t)$ be the output of the neuron subjected to the signal $s(t)$. This output could either be the voltage from Eqs. (1) and (2) in the absence of a threshold, the nonlinear function $F(V(t))$, or the spike train $x(t) = \sum \delta(t - t_i)$ of the spike generating RF and ML models. The Fourier trans-

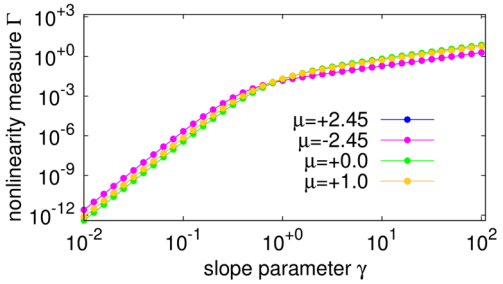

Fig. 3 The nonlinearity measure Γ for the erf static nonlinearities as a function of the slope parameter γ of the static nonlinearity, shown for four different offsets μ for the "resonator cartoon" parameter set of subthreshold voltage dynamics (model parameters are stated in Table 1). Note that the blue curve is identical to the magenta one and hence not visible

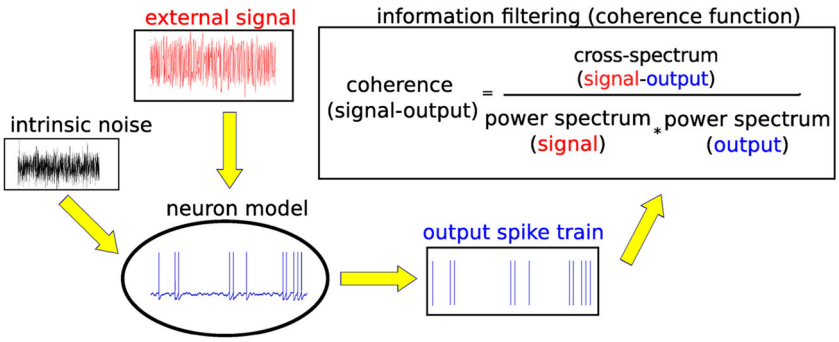

Fig. 4 Scheme of the model analysis. Spikes (output) are generated in response to external stimulation (signal) in the presence of intrinsic noise. Based on signal and output the coherence can be calculated as a frequency-resolved measure of information transmission

formation of the output is denoted by a tilde and is for a finite time window $[0, T]$ defined as

$$\tilde{y}_T(f) = \int_0^T dt\ y(t) e^{2\pi i f t}. \tag{23}$$

Power spectrum of $y(t)$ and cross-spectrum of output- and input-signal are given by

$$S_{\mathrm{y,y}}(f) = \lim_{T\to\infty} \frac{\langle\langle \tilde{y}_T(f)\tilde{y}_T^*(f)\rangle_\xi\rangle_s}{T}, \tag{24}$$

$$S_{\mathrm{y,s}}(f) = \lim_{T\to\infty} \frac{\langle\langle \tilde{y}_T(f)\tilde{s}_T^*(f)\rangle_\xi\rangle_s}{T}, \tag{25}$$

where the star denotes the complex conjugated and the angular brackets indicate ensemble averages over the intrinsic noise $\xi(t)$ and the signal $s(t)$.

For the linear, purely subthreshold model in Section 2.1, all spectra can be calculated analytically. The power spectrum of the voltage fluctuations reads

$$S_{\mathrm{V,V}}(f) = \\ = \frac{\left(\left(\frac{R_\mathrm{L}}{L}\right)^2 + (2\pi f)^2\right)\left(2D + S_{\mathrm{s,s}}(f)\right)/C^2}{\left(\left(\frac{R_\mathrm{L}+R}{RLC}\right) - (2\pi f)^2\right)^2 + (2\pi f)^2\left(\frac{1}{RC} + \frac{R_\mathrm{L}}{L}\right)^2}, \tag{26}$$

while the cross-spectrum between the voltage variable $V(t)$ and the external signal $s(t)$ reads

$$S_{\mathrm{V,s}}(f) = \frac{\left(\frac{R_\mathrm{L}}{L} + 2\pi i f\right) S_{\mathrm{s,s}}(f)/C^2}{\left(\left(\frac{R_\mathrm{L}+R}{RLC}\right) - (2\pi f)^2\right) + (2\pi i f)\left(\frac{1}{RC} + \frac{R_\mathrm{L}}{L}\right)}. \tag{27}$$

Stimulus-response coherence To quantify information transmission between stimulus and spiking response in a frequency-resolved manner—a central point in our study—we turn to the stimulus-response (SR) coherence (see scheme in Fig. 4) and Rieke et al. (1996), Borst and Theunissen (1999), and Roddey et al. (2000). It is defined as

$$C_{\mathrm{y,s}}(f) = \frac{|S_{\mathrm{y,s}}(f)|^2}{S_{\mathrm{y,y}}(f) S_{\mathrm{s,s}}(f)}. \tag{28}$$

The coherence function is a dimensionless squared correlation coefficient, confined to $[0, 1]$. Though not directly applied in this study, it constitutes the ideal linear filter kernel (minimizing the mean squared error), if the stimulus was to be reconstructed from the response. Further, it is related to the lower bound of the mutual information rate (Gabbiani 1996; Borst and Theunissen 1999) by

$$MI_{\mathrm{LB}} = -\int_0^\infty df \log_2\left(1 - C_{\mathrm{y,s}}(f)\right). \tag{29}$$

We note that the integrand, $\log_2\left(1 - C_{\mathrm{y,s}}(f)\right)$, is a monotonic function of the coherence function. Thus, band-pass filter properties of the coherence function coincide with band-pass filter properties of frequency-resolved information transfer.

2.4 Simulation procedures

We numerically simulated the above mentioned neuronal models by using an Euler-Maruyama time discretization algorithm (consult for example Kloeden and Platen 1992) with a time step of 0.1 ms for the RF model and the static nonlinearity and 0.01 ms for the ML model. The statistical measures were obtained by averaging over 10,000 independent trials (120 seconds per trial) with different intrinsic noise and random stimuli. In order to numerically perform the discrete Fourier transformations, we used the FFTW library (Frigo and Johnson 2005). All spectra were then smoothed numerically by using a moving average with a frequency window of 0.5 Hz. All random numbers where generated by using the default generators of the GNU scientific library (Galassi et al. 2009).

3 Results

Understanding signal processing and information transmission at the level of single neurons are important steps in elucidating the mechanisms that govern the functioning of

our brains. We here address a specific question: Does the frequency preference of the *subthreshold* membrane potential also shape the frequency dependence of information transfer in the *spiking* response? In particular, we analyze to what extent a subthreshold resonance of the membrane impedance also results in a band-pass filter of the information transmitted via spikes. We find that the answer is not straightforward: in general, subthreshold resonance is not a guarantee of maximal information transfer in the resonant frequency band. Nonlinearities in neuronal dynamics, however, have a role in "transferring" the subthreshold resonant properties to the frequency dependence of information transfer in the spiking response. To this end, we study the effects of three different nonlinearities on frequency-dependent information transmission. These comprise (1) a fixed threshold and reset (as commonly applied in integrate-and-fire and resonate-and-fire type models), (2) the nonlinearity in the differential equations of the conductance-based Morris-Lecar model, and (3) a static nonlinearity applied to linear, subthreshold dynamics. In the following, information transfer and its frequency dependence is analyzed for these three conceptually different models.

To lay the ground, we begin with an analytical and numerical investigation of the information filtering properties of linear resonant neurons described by Eqs. (1) and (2) (see Section 3.1). Thereafter, we concentrate on the impact of a *discontinuous nonlinearity* implemented by a fire-and-reset rule onto the resonant subthreshold dynamics governed by Eqs. (1) and (2) (see Section 3.2). Following these extensive numerical studies, we analyze the Morris-Lecar model with its *continuous nonlinearity* (see Section 3.3). We conclude our study with a detailed numerical analysis of a more artificial model—a static, sigmoidal nonlinearity applied to the linear resonant dynamics (see Section 3.4).

3.1 Subthreshold resonant voltage dynamics, if linear, do not show a resonance in information transfer

The resonate-and-fire model is a well-established model for neurons with a subthreshold resonance. It is particularly simple in its subthreshold dynamics, which are linear. The full model includes a fire-and-reset rule that renders the spiking dynamics strongly nonlinear. Here, we first turn to the pure subthreshold dynamics in the absence of a threshold before we move on to the full spiking dynamics. To analyze information transfer and its frequency dependence, we calculate the stimulus-response coherence (see Section 2.3).

Power and cross-spectra of the membrane voltage and the signal $s(t)$ (given by the Ornstein-Uhlenbeck process, see Eq. (5) in Section 2) can be calculated via the Rice method (Rice 1944; Risken 1984), and are given in Section 2 by Eqs. (26) and (27). Based on Eq. (28), we hence obtain the exact expression for the coherence between the membrane voltage and the stimulus $s(t)$ in the absence of a threshold:

$$C_{\mathrm{V,s}}(f) = \frac{1}{1 + \frac{D}{D_{\mathrm{OU}}}\left(1 + (2\pi\tau_{\mathrm{ou}} f)^2\right)}. \tag{30}$$

At first glance surprising, the coherence is a strictly monotonically decreasing function of frequency. This observation is in marked contrast to the resonances exhibited by the impedance as well as power and cross-spectra. One could be tempted to draw the conclusion that high power comes along with high information transmission, described by the coherence function. However, as Eq. (30) proves, this intuition is not correct. This effect can be understood if one keeps in mind that the coherence is essentially given by the ratio of two functions (squared cross-spectrum and output power spectrum). Both functions exhibit peaks at about the same frequency; in the coherence function these peaks cancel each other. The remaining low-pass dependence on frequency is explained by the fact that the stimulus power of the Ornstein-Uhlenbeck process decreases with frequency, whereas the white background noise does not. Hence, the coherence function of the linear resonator model without threshold is shaped by the statistics of the input signal and the intrinsic noise, but not by the model's resonator properties. As a consequence, our measure of band-pass information filtering, the quality factor Q_{C}, attains its minimal value of one:

$$Q_{\mathrm{sub,C}} = 1 \quad \text{(without threshold)}, \tag{31}$$

implying a low-pass filter on information.

For the special case of the linear system driven by Gaussian noise and signal, the lower bound formula Eq. (29) combined with Eq. (30) yields the exact value of the lower bound of the mutual information rate (without threshold) and reads:

$$MI_{\mathrm{sub,exact}} = \frac{\sqrt{1 + D_{\mathrm{OU}}/D} - 1}{2\ln(2)\tau_{\mathrm{OU}}}. \tag{32}$$

This result illustrates again that the information transfer of the linear system does not depend on resonance properties of voltage dynamics but only on the input's signal-to-noise ratio D_{OU}/D as well as the input's signal timescale τ_{OU}.

3.2 Combination of linear resonant dynamics with a threshold "recovers" a resonance of information transfer by spikes

We now turn to the full spiking dynamics of the RF model and combine the linear subthreshold dynamics, described by Eqs. (1) and (2), with a fire-and-reset rule, which renders the model nonlinear. As we will see, the addition of this simple nonlinearity to the linear model (discussed in the previous section) results in a bandpass of information transfer

by spikes if the subthreshold voltage dynamics are resonant. How pronounced this effect is, depends on the mean of the input current (or, mathematically, the fixed point V_{FP}). In the following sections we explore the dependence of spiking information transmission on the strength of the signal, D_{OU}, as well as the voltage reset and the refractory period.

Because Eq. (30) is no longer applicable in the spiking regime, we employ extensive numerical simulations (see Section 2) of the stochastic differential equations to determine the spectral coherence function for more than 75.000 parameter sets. For illustration purposes, we concentrate on the results for three distinct parameter sets given in Table 1, which represent three qualitatively different neuron models that exhibit: an extremely strong subthreshold resonance (termed "resonator cartoon"), a more realistic subthreshold resonance (termed "stellate cell"), or a nonresonant membrane impedance (termed "pyramidal cell"). The resonator cartoon model shows an unphysiologically high impedance resonance (characterized by a quality factor Q_Z of about 16). Parameters of stellate and pyramidal cell models have previously been adapted to experimental data of cells in the entorhinal cortex (Schreiber et al. 2004). The stellate cell model has a resonance with $Q_Z \approx 2$, the pyramidal cell model is nonresonant. The latter model cell is hence an integrator (Izhikevich 2007) and to first approximation equivalent to an integrate-and-fire type model. The output characteristics of the subthreshold voltage at these three parameter sets in the absence of a threshold are given in Table 2.

In Table 1 (below the dashed line), we also provide the values of the input parameters, the choice of which is described in the following. If we want to compare the model at distinct parameter sets, the question arises how to choose the stimulus parameter values in order to make the comparison meaningful. Here, we used values of the DC input I_0 that gave rise to similar firing rates in all three cases; for the values, see Table 3. Furthermore, for the two stochastic processes $\eta(t)$ (intrinsic noise) and $s(t)$ (signal), we chose the values of the noise intensities such that the total variance of the voltage without threshold was approximately equal in all three cases. This resulted in similar values of the coefficient of variation CV $\in [0.6, 0.8]$; see Table 3. The fraction contributed by the signal to the voltage variance was chosen to be 2/3. For the signal we used in all cases a correlation time $\tau_{OU} = 10$ ms.

In Fig. 5 we show the spectral statistics of the RF neuron spiking responses for the three selected parameter sets: the coherence function (a1, b1, c1), the cross-spectrum (a2, b2, c2), and the spike train power spectrum (a3, b3, c3). In all three sets, power and cross-spectra reveal peak around 8 Hz. However, only for the resonant parameter sets (Fig. 5a1, b1) we observe a peak in the coherence function, indicating a band-pass filter of information. For the nonresonant (integrator) neuron (c1), the coherence decays monotonically. Whether the coherence shows a maximum at a non-vanishing frequency (values given in Table 3), depends on the squared cross- and power spectra; we recall that the coherence is the ratio of these two functions.

In Fig. 5a1, b1, c1 we also compare the coherence of the spiking neuron model to the voltage-input-coherence in the absence of a threshold, given in Eq. (30). As can be expected, the nonlinearity of spike generation reduces the coherence at all frequencies accompanied by an overall reduction of information rate (cf. Tables 2 and 3). This is true for both resonant and nonresonant neurons and is most pronounced for the resonant cells (a1, b1) at low frequencies ($f < 10$ Hz). The effect results from a combination of the resonance in the subthreshold voltage dynamics and the nonlinearity of spike generation.

Regarding the characteristics of the resonance, we note that the coherence is maximized at frequencies that are not

Table 2 Characteristics of the dynamics (above the dashed line) and of information filtering (below the dashed line) in the linear, purely subthreshold RF model (without threshold)

Parameter	Resonator cartoon	Stellate cell (EC-II)	Pyramidal cell (EC-III)
$f_{\text{nat}}\ [Hz]$	7.6	7.99	*none*
$f_{\text{res}}^{\text{Z}}\ [Hz]$	9.5	8.9	*none*
Q_{Z}	12.1	1.5	1.0
$f_{\text{res}}^{\text{sub,C}}\ [Hz]$	0.0	0.0	0.0
$Q_{\text{sub,C}}$	1.0	1.0	1.0
$MI_{\text{sub,exact}}$ $[bits/s]$	145.26	143.49	116.66

Top to bottom below the dashed line: frequency of maximal coherence of the subthreshold voltage response, quality factor of this coherence, mutual information rate *MI*

Table 3 Characteristics of firing (above the dashed line) and coherence of the spiking response (below the dashed line) for the RF model (with threshold) with OU stimulation

Parameter	Resonator cartoon	Stellate cell (EC-II)	Pyramidal cell (EC-III)
Firing rate [Hz]	3.78	3.92	3.70
CV	0.78	0.70	0.63
$f_{\text{spike, C}}\ [Hz]$	9.3	8.17	0
$Q_{\text{spike, C}}$	40.8	1.6	1.0
$MI_{\text{spike, LB}}$ $[bits/s]$	9.80	10.05	8.35
	6.7 $\%MI_{\text{sub}}$	7.0 $\%MI_{\text{sub}}$	7.2 $\%MI_{\text{sub}}$

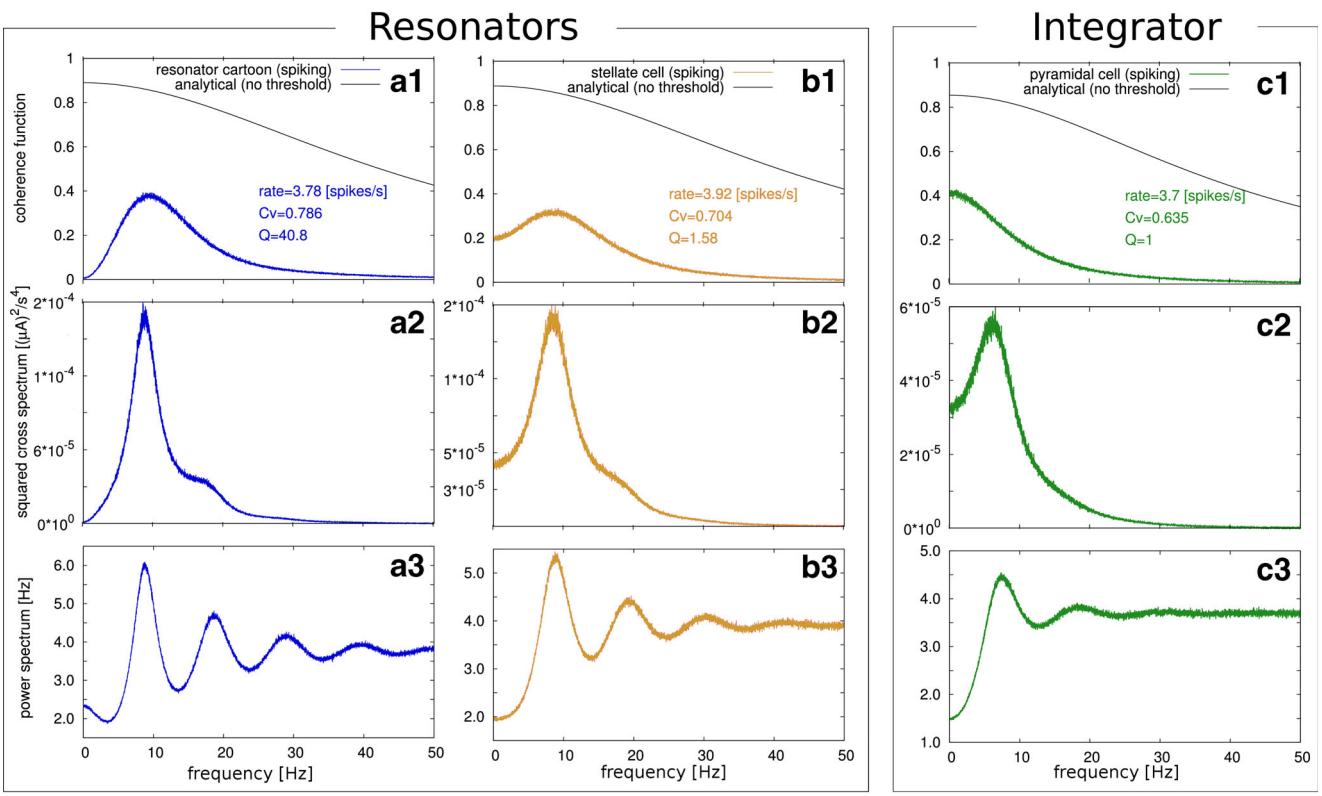

Fig. 5 Examples of spectral functions relating to information transmission in the RF model. Coherence for the "resonator cartoon" (**a1**), stellate cell (**b1**) and pyramidal cell (**c1**). The theoretical results (*black solid lines* in **a1**, **b1**, **c1**) for the purely subthreshold dynamics (without fire-and-reset) are given in Eq. (30). Cross-spectra between the input (OU-process) and the output spike train for the resonator cartoon model (**a2**), the stellate model (**b2**), and for the pyramidal model (**c2**). Power spectra of the output spike trains are shown in (**a3**), (**b3**), and (**c3**), respectively (model parameters as listed in Table 1)

identical but close to the ones that maximize the response to a ZAP current (cf. Tables 3 and 2). Furthermore, for the stellate cell model, the quality factor Q_Z of the response to a ZAP-current and that of the coherence function Q_C are similar. For the resonator cartoon, the coherence function has more than twice as large a quality factor Q_C compared to the impedance quality Q_Z. Apparently, there is in general no simple relation between these measures of information and power filtering.

3.2.1 DC input I_0 affects the frequency dependence of information transfer by spikes

The fixed point V_{FP} of the purely subthreshold voltage dynamics in the RF model depends on the DC input I_0, see Eq. (3). Firing statistics and signal transmission properties are determined by the position of this fixed point relative to the threshold. Next, we hence inspect firing rate, CV and the characteristics of information transmission as functions of the fixed point.

First of all, the firing statistics of the model for all three parameter sets behave as can be expected. As the fixed point approaches and passes the threshold, the firing rate increases (Fig. 6a) and the coefficient of variation drops (Fig. 6b). For a fixed point far from threshold, the firing rate is exponentially small (inset Fig. 6a) and the CV is close to the Poissonian limit $CV \approx 1$ of rare-event statistics.

The lower part of Fig. 6 displays information theoretic measures of interest as functions of the fixed point. Our measure for the peakedness of the coherence function, Q_{C}, is for the resonant versions of the model clearly maximal for a fixed point well below the threshold. That means that it is maximal in the regime of irregular low-frequency firing. The resonator cartoon achieves in this limit quality values close to one hundred while the stellate cell is limited to a maximal Q_C of 2.2 (Fig. 6c). We also note here that even if the fixed point of the subthreshold dynamics without threshold, V_{FP}, is slightly above the threshold of the full spiking model, we observe a band-pass filter effect on information for resonant neurons (see Fig. 6c). Although diminished, the band-pass filter property on information is still present for resonant neurons within this mean-driven firing rate regime. For DC values well above the threshold value, however, the coherence exhibits low-pass properties. For the model versions and range of V_{FP} below the threshold, for which we observe a pronounced band-pass information filter, the

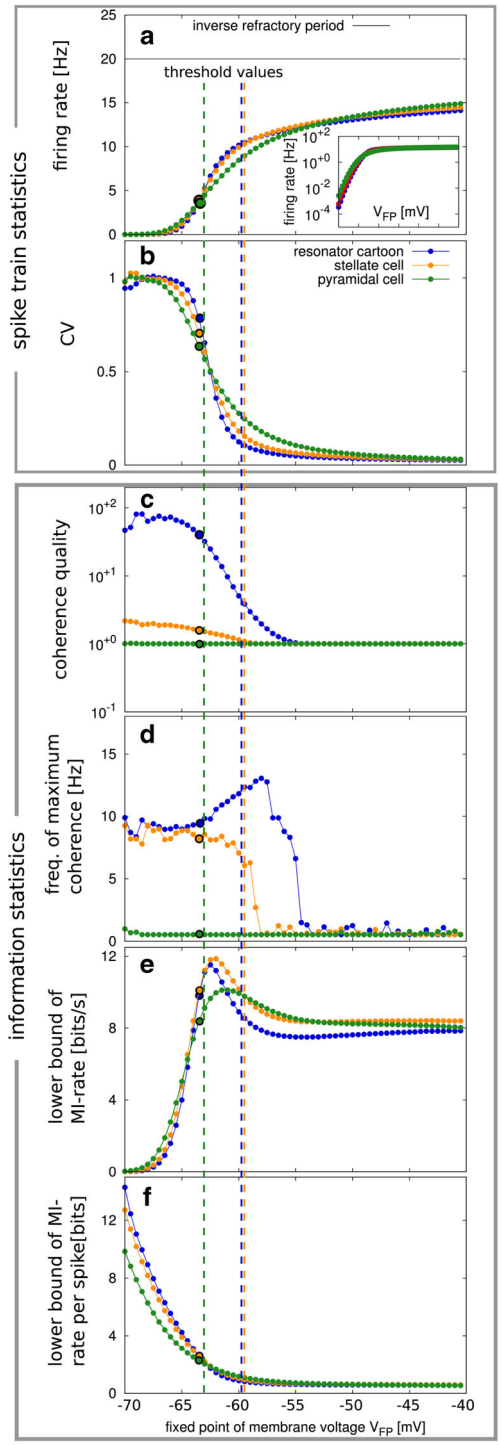

Fig. 6 The DC input I_0 sets the fixed point V_{FP} of the linear, subthreshold voltage dynamics. Characteristics of firing and information transmission depend on V_{FP}: **a** firing rate, **b** coefficient of variation, **c** coherence quality, **d** frequency of maximum coherence, **e** lower bound of the mutual information rate, and **f** lower bound of the mutual information rate per spike. *Colored solid lines* correspond to the three illustration RF parameter sets; *dashed lines* indicate threshold values of the models (stated in Table 1). *Dots with black margin* correspond to values of I_0 as listed in Table 1, corresponding spectra shown in Fig. 5

peak frequency of the coherence (Fig. 6d) is close to the resonance frequency of the impedance function without threshold. In marked contrast to the resonant cells, the pyramidal cell model has a coherence quality factor Q_C of one for all V_{FP}, showing that the nonresonant (integrator) cell cannot act as a band-pass filter of information irrespective of the fixed point position.

The overall dependence of the information rate on the fixed-point (Fig. 6e) shows the following characteristics. For fixed-points far below the threshold, the information rate is very low because the firing rate is very small (Borst and Theunissen 1999) although the information rate *per spike* can still be high (Fig. 6f). Upon increase of V_{FP}, the information rate grows steeply, reaches a maximum at a fixed-point still below threshold, and then saturates at a value of about 8 bits/s, similar for all parameter sets. The existence of the maximum and the plateau depends strongly on the absolute refractory period τ_{abs}; without refractory period the information rate increases monotonically in this range (not shown). Moreover, the incorporation of an absolute refractory period even leads to a decay of the information rate (for much larger values of the fixed point, see Fig. 6e). In this limit the neuron's firing is largely determined by the refractory period alone ($r \to \tau_{\mathrm{abs}}^{-1}$) and cannot encode information about the stimulus any more. One important conclusion that we can draw from Fig. 6e and f is that the total information flow is similar for all three parameter sets in spite of very different information filtering properties, as illustrated in Fig. 6c. This implies that from the dependence of the total information rate on the fixed-point alone we cannot distinguish an integrator from a resonator cell.

As already pointed out, in the limit of low firing rate, where band-pass filtering of information for the resonator cells is most pronounced, the overall information rate at all parameter sets is extremely small (Fig. 6f). However, if we choose a fixed-point around the value indicated by the marked data points in Fig. 6 (corresponding to the parameters used in Fig. 5) we see that the information rate has already reached a large fraction of its overall maximum while the coherence quality is still significantly larger than one. Thus, it is possible to achieve a band-pass filter of information that still transmits at reasonable information rates.

3.2.2 Signal strength D_{OU} influences the frequency-dependence of information filtering in resonant neurons

Neurons receive stimulation with signals of different intensities. For this reason we next address how the band-pass filtering properties of information are affected by the strength of the stochastic stimulus $s(t)$.

Firing rate and coefficient of variation CV depend on the signal strength at a subthreshold baseline current I_0 (excitable regime) as described in the following. The firing rate increases with the stimulus intensity D_{OU} (Fig. 7a) because fluctuations accelerate the escape to the threshold as it is typical in excitable systems (Lindner et al. 2004). The behavior of the CV (Fig. 7b) is at the first glance surprising because this measure of output irregularity decreases monotonically with increasing signal intensity. This behavior can be understood by the comparatively long refractory period, which can result in such a drop (Lindner et al. 2002).

The dependence of the coherence quality on the strength of our input signal (Fig. 7c) is similar to the dependence on the fixed point (Fig. 6c) at small input signal we observe a maximum Q_C close to one hundred for the resonator cartoon and of about two for the stellate cell. With increasing amplitude of the OU-process Q_C approaches one, i.e. the value that indicates a lack of band-pass filtering of information. As expected, the integrator cell shows $Q_C = 1$ for all signal amplitudes.

Figure 7d displays the peak frequency of the coherence and demonstrates that for small and moderate input strengths the band-pass filter on information is centered around the resonance frequency of the impedance. By increasing the signal amplitude, we both increase the output firing rate as well as the input signal-to-noise ratio D_{OU}/D. Hence, we can expect that the information rate, at least initially, goes up with growing D_{OU} as confirmed in Fig. 7e.

The inset in this panel (in Fig. 7e) indicates that at large signal amplitude the information rate drops again with increasing amplitude. In this limit the spike train's interspike intervals largely reflect the absolute refractory period and cannot encode much about the time-dependent stimulus. We note that the information per spike (Fig. 7f) is again maximal in the limit of low firing rate, i.e. here for small signal amplitude.

We conclude that increasing the signal strength has a qualitatively similar effect like the variation of the DC input discussed in the previous section. A band-pass filter on information for resonant neurons can be achieved at low-to-moderate input signal-to-noise ratio and low-to-moderate firing rate. The regime of tonic firing at high rates is apparently always associated with low-pass filtering of neuronal information.

For most values of the signal strength, D_{OU}, in our simulation results, the signal was significantly stronger than the intrinsic noise. This becomes apparent by the strong dependence of the mean firing rate on the signal amplitude (Fig. 7a), which indicates that the system operates in a nonlinear response regime. Only for very small strength, D_{OU}, and exponentially small firing rate (i.e. at the left end of Fig. 7) the system is in the *linear response regime*, where

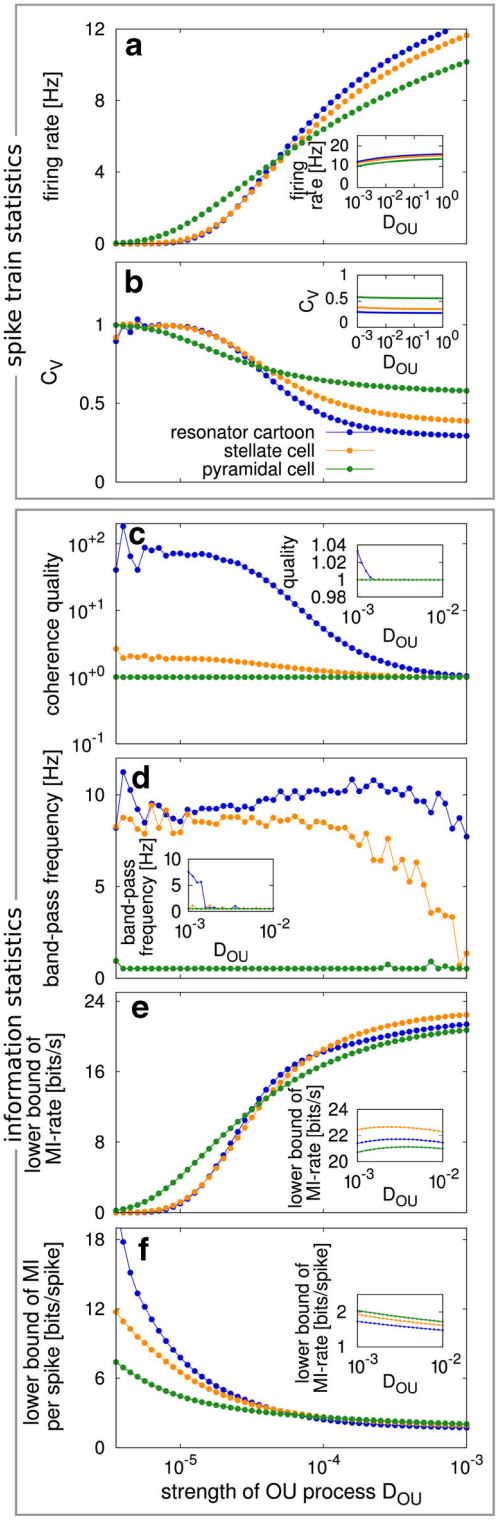

Fig. 7 Characteristics of firing and information transmission depend on the strength of the external signal D_{OU}: **a** firing rate, **b** coefficient of variation, **c** coherence quality, **d** frequency of maximum coherence, **e** lower bound of mutual information rate, and **f** mutual information rate per spike. *Different colors* correspond to models as in Fig. 6. Insets extend the respective statistics for larger D_{OU}

the signal merely imposes a weak modulation of the instantaneous firing rate. In this regime the coherence can be simplified as follows

$$C(f) = \frac{|S_{xs}|^2}{S_{xx}S_{ss}} \approx \frac{|\chi S_{ss}|^2}{S_{xx}S_{ss}} = \frac{|\chi|^2}{S_{xx}} S_{ss} = \frac{|\chi|^2}{S_{xx}} \frac{2D_{\mathrm{OU}}}{1+(2\pi f \tau_{\mathrm{ou}})^2}. \quad (33)$$

In the first step we expressed the cross-spectrum by the rate-modulation factor $\chi(f)$, the so-called susceptibility (Fourier transform of the linear response function) and we inserted the power spectrum of the OU process in the last step to reveal the dependence on D_{OU}. One important condition for this approximation is that the spike-train power spectrum S_{xx} (also appearing as a factor in the denominator) is close to the spontaneous power spectrum (the spectrum for $\eta(t) \equiv 0$) and thus largely independent on the signal, but that is the case for our model if the signal is sufficiently weak.

The linear-response approximation Eq. (33) tells us, that for weak signal strength the *shape* of the coherence, i.e. its dependence on frequency, is independent on D_{OU}. Consequently, all measures derived from this frequency dependence, such as the the quality of the filter or the frequency at which the coherence attains its maximum, should be independent of D_{OU}. This is indeed observed in Fig. 7c, d for $D_{\mathrm{OU}} < 10^{-5}$ and thus indicates the regime of linear response for this particular choice of parameters.

In Richardson et al. (2003) an approximation for the susceptibility $\chi(f)$ of a generalized integrate-and-fire neuron has been calculated. Although this model differs from ours by the specific reset rule, comparison to simulations reveals that the cross-spectrum of our model can be well described by the analytical approximation from Richardson et al. (2003) provided the signal amplitude D_{OU} is sufficiently small. Unfortunately, the cross-spectrum alone is not sufficient to calculate the frequency-dependence of the coherence. The latter also is strongly shaped by the spike-train power spectrum, the calculation of which poses a nontrivial and so far unsolved theoretical problem. Thus, more efforts are needed to characterize the information-filtering effect analytically in the linear-response regime.

3.2.3 Resonant information transfer does not strongly depend on reset value and absolute refractory period

Two important neural parameters that vary among neurons are the reset value V_{reset} (reflecting the depth of after-hyperpolarization) and the absolute refractory period τ_{abs}. Commonly, the reset value is thought to be related to a relative refractory period, because starting further away from threshold will prevent early spikes (i.e. short interspike intervals). In the resonate-and-fire model we will see below that a variation of the reset has also other consequences. Regarding the absolute refractory period, we note that it can be up to a few ten milliseconds in stellate cells (Engel et al. 2008). In the following, we explore whether a change in these parameters (that are related to the nonlinearity in the model) affects and potentially diminishes information filtering.

If we change the reset value V_{reset}, also the initial value of the current variable is affected (see Eq. (13) in Section 2) and it is not straightforward to predict, how this in turn influences spike train statistics. Somewhat surprisingly for the excitable regime considered here, a stronger hyperpolarization (more negative reset value) results in a *higher* firing rate. This can be understood as a rebound effect, typical in resonator neurons (Izhikevich 2007). For our example in Fig. 8a, a stronger hyperpolarized initial value brings the deterministic trajectory closer to threshold and thus increases the probability of spiking for the stochastic trajectory. Because the amplitude of the coherence is known to depend strongly on the firing rate, one could expect that changing the reset point will hence affect the information transmission properties of the neuron model.

In Fig. 8a we show the effect of lowering V_{reset} on the coherence, the cross-spectrum, and the power spectrum, respectively. Both cross- and power spectra become more narrow upon lowering of the reset point. However, contrary to our expectation above, the shape of the coherence is affected weakly and shows in all cases a peak at the same frequency close to f_{res}. The overall amplitude of the coherence and thus the information rate only slightly drops when shifting V_{reset} to more hyperpolarized values (see numerical values in Fig. 8a1).

The effect of an increase of the absolute refractory period on spectral measures is illustrated in Fig. 8b. The firing-rate statistics and hence the power spectrum as well as the cross-spectrum are strongly influenced by the absolute refractory period (see Fig. 8b2, b3 and numerical values in Fig. 8b3). The location of peaks is drastically changed when increasing τ_{abs} from a few tens to up to one hundred ms. However, the coherence is not affected in its shape but only in its amplitude, which declines with increasing refractory period. This overall reduction can be accounted for by the decline in firing rate (not shown).

We conclude that variations of the reset point and of the absolute refractory period have little effect on the shape of the information filter but only affect the absolute information rate. This observation holds despite the pro-

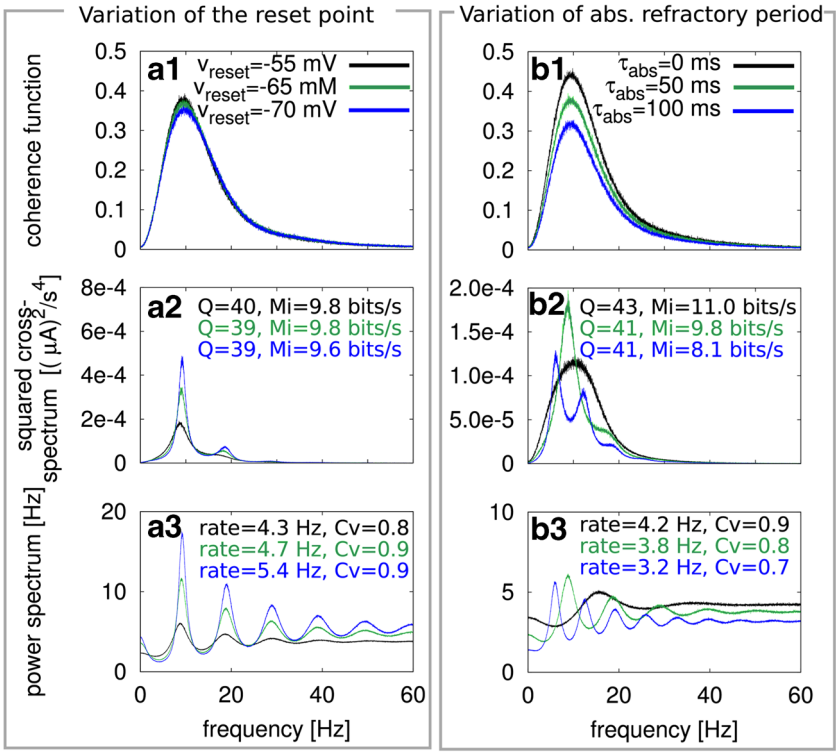

Fig. 8 **a** Dependence of information transmission on the voltage reset in the RF model. Influence of V_{reset} on the coherence function (**a1**), cross-spectrum (**a2**), and power spectrum (**a3**). **b1**–**b3** Influence of the absolute refractory period on the same functions. Variations are placed in the vicinity of the standard parameters of the resonator cartoon parameter set (stated in Table 1)

nounced influence of these parameters on the power and cross-spectra. Hence, information filtering properties of the resonate-and-fire model are robust under variation of the refractory parameters within their physiological ranges.

3.2.4 Impedance resonance coincides with a resonance in spike-based information transfer for a broad range of parameters

In Section 3.2 we saw that the band-pass filter on information is only observed in the resonate-and-fire model if its subthreshold impedance has a pronounced peak, i.e. in the presence of a resonance but *not* in the limit of an integrator. Next, we explore the relation between the subthreshold impedance quality Q_Z (a measure of the resonance property of the model) and the quality of the coherence $Q_{\text{spike,C}}$ (a measure of information filtering) over a wide range of parameters. To this end, we systematically change the quality value of the impedance function (keeping the resonance frequency f_{res} fixed) by changing R, R_L, L in a way detailed in Appendix A.1. Secondly, for each value of impedance quality in the range between 1 and 10, we vary the output firing rate between $0.5 - 15$ Hz by changing the DC I_0; note that due to the absolute refractory period of 50 ms the output firing rate is bounded by 20 Hz.

For the standard resonance frequency of $f_{\text{res}} = 9.5$ Hz, Fig. 9 depicts the quality of the coherence versus the quality of the impedance. If we do not further constrain the data, different parameter combinations uniformly fill the plane. The left upper region forms an exception, implying that low impedance quality (a regime close to that of a nonresonant

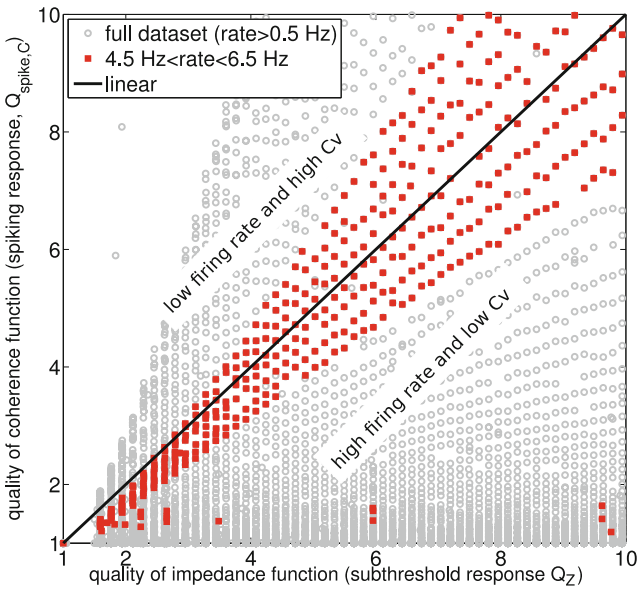

Fig. 9 Correlations between coherence quality of the spiking system (with threshold) and the impedance quality of the linear system (without a threshold) by varying the subthreshold impedance quality with fixed resonance frequency of 9.5 Hz as described in Appendix A.1. Marked (*red*) data points highlight a data subset constrained to firing rates in [4.5; 6.5] Hz

integrator neuron) cannot result in pronounced information filtering.

If we sort the data according to the output firing rate, a simple relation between impedance quality and coherence quality emerges. For firing rates between 4.5 and 6.5 Hz, we find that most points scatter around the diagonal, i.e. for these output firing rates $Q_{\mathrm{spike,C}} \approx Q_{\mathrm{Z}}$. Lower firing rates yield points above the diagonal ($Q_{\mathrm{spike,C}} > Q_{\mathrm{Z}}$) while for higher firing rates the band-pass filter property is diminished ($Q_{spike,C} < Q_{\mathrm{Z}}$).

As demonstrated in Figs. 10 and 11 we find an essentially similar behavior for lower ($f_{\mathrm{res}} = 5$ Hz, Fig. 10) or higher resonance frequency ($f_{\mathrm{res}} = 15$ Hz, Fig. 11). The only marked difference lies in the range of firing rates for which both quality factors are roughly equal: for the lower resonance frequency, we find $3 < r < 4.5$ Hz (see Fig. 10), while at the higher resonance frequency, $5 < r < 8$ Hz (see Fig. 11).

To conclude, the band-pass filtering of information is a robust property of the resonate-and-fire model that can be observed in a wide range of output firing rates as long as the subthreshold resonance of the model is pronounced.

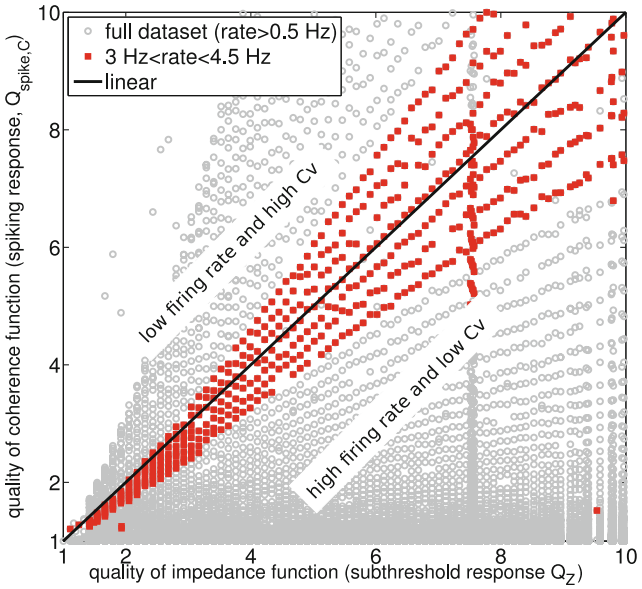

Fig. 10 Correlations between coherence quality of the spiking system (with threshold) and the impedance quality of the linear system (without a threshold); as in Fig. 9, but for a fixed resonance frequency of 5 Hz. Marked (*red*) data points highlight a data subsets constrained to firing rates in [3; 4.5] Hz

3.3 The Morris-Lecar model with subthreshold impedance resonance also exhibits a resonance of spike-based information transfer

Next, we turn to a second type of model, which generates action potentials directly from the dynamical equations of voltage and a gating variable and does not require a fire-and-reset rule: the Morris-Lecar model in its formulation by Rinzel and Ermentrout (1989) given in Section 2.1.3. The model is defined by a two-dimensional system of differential equations that directly include the nonlinearity. Depending on the choice of parameters, this spiking neuron model can exhibit type I or type II dynamics with spike initiation via a saddle-node on an invariant circle bifurcation or a subcritical Hopf bifurcation, respectively, see also Rinzel and Ermentrout (1989). Here, we inspect whether the information filtering effect is also present in this biophysically more realistic resonant neuron.

In order to compare the coherence function for resonant and nonresonant (integrator) versions of the model, we choose parameter sets used before by Rinzel and Ermentrout (1989) (see Table 4). The type I parameter set corresponds to a nonresonant neuron, the type II parameter set to a resonant neuron. For both parameter sets we choose the DC I_0 and the intensity of the driving fluctuations (signal and intrinsic noise) such that we obtain similar values for the firing rate and CV, which are stated in Fig. 12c. Under these conditions, the resonant type II parameter set (yellow ocher in Fig. 12a) displays a peak in the coherence located close to the resonance frequency of the subthreshold response. As found for the resonate-and-fire model, the ML model poised in a regime of subthreshold resonance acts

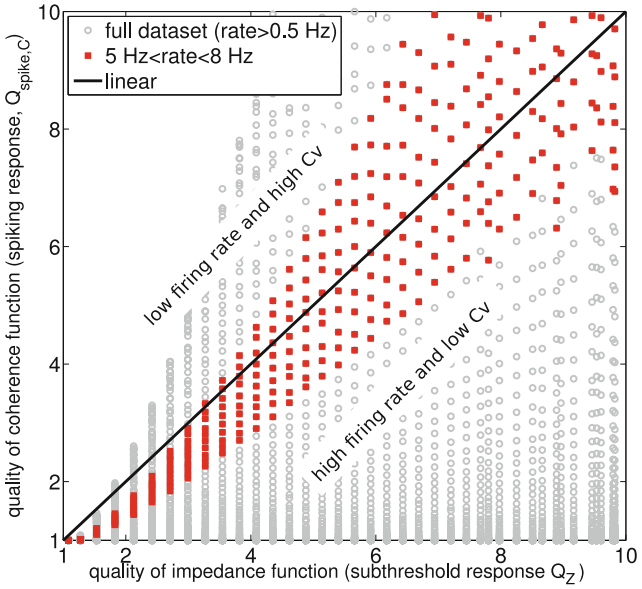

Fig. 11 Correlations between coherence quality of the spiking system (with threshold) and the impedance quality of the linear system (without a threshold); as in Fig. 9, but for a fixed resonance frequency of 15 Hz. Marked (*red*) data points highlight a data subsets constrained to firing rates in [5; 8] Hz

Table 4 Morris-Lecar (ML) model parameters (Schreiber 2004) and characteristics of firing and information transmission (below the dashed line)

Parameter	Type II (resonator)	Type I (integrator)
$V_1\ [mV]$	-1.0	-1.0
$V_2\ [mV]$	$+15$	$+15$
$V_3\ [mV]$	$+0$	$+10$
$V_4\ [mV]$	$+30$	$+14$
$g_{\mathrm{Ca}}\ [mS/cm^2]$	1.1	1.1
$g_K\ [mS/cm^2]$	2.0	2.0
$g_L\ [mS/cm^2]$	0.5	0.5
$E_{\mathrm{Ca}}\ [mV]$	$+100$	$+100$
$E_K\ [mV]$	-70	-70
$E_L\ [mV]$	-50	-50
$C\ [\mu F/cm^2]$	1	1
ϕ	$\frac{1}{5}$	$\frac{1}{3}$
$I_0\ [\mu A/cm^2]$	20.21	7.252
D	5.0	10.0
D_{OU}	5.0	2.0
$\tau_{\mathrm{OU}}\ [ms]$	1.0	10.0
rate [Hz]	4.46	4.40
CV	0.94	0.92
$f^{\mathrm{coherence}}\ [Hz]$	59.2	none
Q_{spike}	4.2	1.0
Q_{sub}	1.0	1.0
$MI_{\mathrm{LB}}^{\mathrm{spike}}$ [bits/s]	16.7	9.4
$MI_{\mathrm{LB}}^{\mathrm{sub}}$ [bits/s]	520.2	75.4

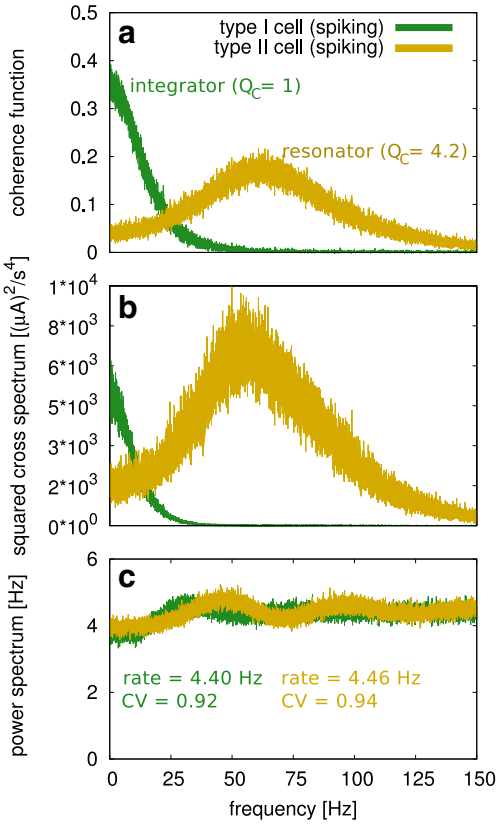

Fig. 12 Spectral measures for the Morris-Lecar model (with parameters as in Table 4). **a** Coherence function for type I (*black*) and type II (*yellow ocher*) neuron models. **b** Cross-spectra between the input-signal (OU-process) and the output (spike train). **c** Power spectra of the output spike train

as a band-pass filter on information. In contrast to this, the coherence function of the type I integrator model (black in Fig. 12a) decays monotonically with frequency. Hence, the ML model in the regime with nonresonant subthreshold membrane impedance can be regarded as a low-pass filter on information.

The mechanism for the occurrence of the coherence peak at non-vanishing frequency is similar to one we have observed for the resonate-and-fire model. In the resonant model, both power spectrum (Fig. 12b) and cross-spectrum (Fig. 12c) possess peaks at the resonance frequency, only that the peak in the cross-spectrum is more pronounced. For the nonresonant model, there is no peak in the cross-spectrum and only a hump in the power spectrum and their ratio does not exhibit a maximum. Our simulations at other parameter values in the type I regime indicate that even with a lower CV (resulting in peaked cross-spectrum) the coherence function is still maximal at zero frequency, i.e. at acts as a low-pass information filter. We note here that we also studied the properties of the information filtering characteristics of the ML model by varying the baseline current I_0 as well as the input-signal strength D_{OU}. The results were similar to the results of the resonate-and-fire neuron model (data not shown).

We conclude that the Morris-Lecar model, if poised in a regime with subthreshold resonance, acts as a band-pass filter on information close to its subthreshold resonance frequency. Thus, the band-pass filtering of information is not an artefact of the specific fire-and-reset rule in the resonate-and-fire model.

3.4 Also static nonlinearities lead to a bandpass in information transfer in cells with subthreshold impedance resonance

As we have seen, both types of nonlinearities—fixed threshold and conductance-based spike generation—translate a

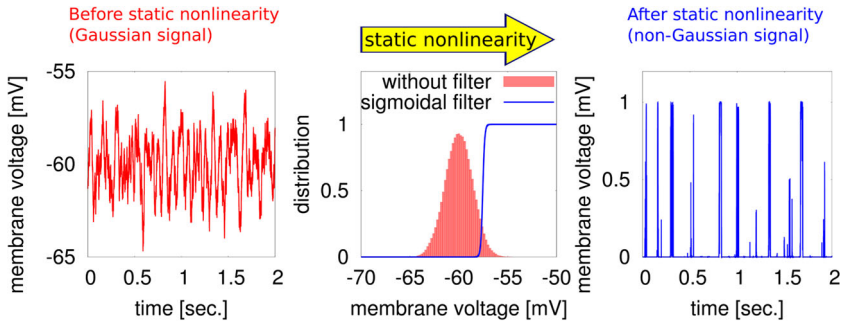

Fig. 13 Schematic representation of the model with static nonlinearity. Voltage traces are obtained from the linear subthreshold dynamics (*left panel*) and then passed through the static nonlinearity (*middle panel, blue line*) to obtain the output signal (*right panel*). The voltage distribution (*in red*) relative to the static nonlinearity is depicted in the *middle panel*. Parameters of the nonlinearity: steepness $\gamma = 100.0$ and offset $\mu = 2.45$ mV

subthreshold resonance to a peaked spectral coherence (and hence a peaked frequency dependence of spike-based information transmission) in the same range of frequencies. To test whether general types of nonlinearities also can produce this effect, we next turned to an artificial system where the subthreshold voltage response of the linear system (generated by the subthreshold dynamics of the resonate-and-fire model) is merely passed through a sigmoidal, static nonlinearity (Fig. 13).

Transforming the linear response V by the static nonlinearity F yields $F(V)$. For very steep nonlinearities, resembling a Heaviside function, the system's output can be pulsatile (see Fig. 13). A spectrally resolved coherence function of the output of this nonlinear system shows a clear resonant peak (Fig. 14, blue curve). For comparison, in Fig. 14 also the coherence of the corresponding (linear) voltage responses V (black curve) and the coherence of the spike responses of a resonate-and-fire neuron with identical subthreshold dynamics (green curve) are depicted. Coherence functions of the static nonlinearity model and the resonate-and-fire model both peak in the range of the subthreshold resonance of the membrane impedance. Parameters of the static nonlinearity have been tuned to maximize similarity of the coherence functions of the resonate-and-fire neuron model (with threshold) and the coherence function of the output after the sigmoidal static nonlinearity (see Fig. 14).

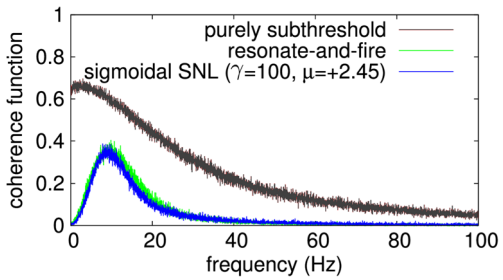

Fig. 14 Coherence function of the resonator cartoon model without threshold (*black line*), with threshold-and-reset (*green line*), and the model with sigmoidal static nonlinearity (*blue line*). Parameters of the sigmoidal nonlinearity as in Fig. 13; μ equals the distance between voltage fixed point V_{FP} and threshold V_{thresh} of the resonator cartoon parameter set (see Table 1)

3.4.1 Coherence shape and mutual information rate depend on the nonlinearity

The shape of the spectral coherence and the lower bound of the mutual information rate depends on the relative location of the distribution of voltages, V, with respect to the static nonlinearity. Covering values from 0 to 1, the nonlinearity is defined by two parameters: the slope factor γ and the offset value μ (specifying the location inversion point relative to the mean of the voltage distribution before it is passed through the nonlinearity). For details see Section 2.2. For a given distribution of the linear voltage responses, systematic variation of the relative location of the nonlinearity with respect to the voltage distribution modifies the peakedness of the spectral coherence function (Fig. 15a) as well as the mutual information rate (Fig. 15b). The coherence is peaked least when the nonlinearity's inflection point coincides with the mean of the voltage distribution, i.e. when the voltages mainly fall into the relatively linear range of the sigmoidal. When shifting the inflection point of the sigmoidal, however, the peakedness of the spectral coherence (i.e. coherence quality) rises symmetrically to both sides. In analogy to the negative correlation between coherence quality and information rate observed in the previous sections, information rate is the larger, the lower the peakedness of the spectral coherence (Fig. 15b).

Both statistics are symmetric with respect to μ. The coherence quality (a) shows a maximum at γ-dependent off-

set μ and approaches the low-pass filter $Q_C = 1$ at very large offsets from the mean value (0 mV) of the linear system. The mutual information rate (b) is always maximal for offsets μ equal to the mean value of the linear system and decreases monotonically to zero, because the coherence function is drastically reduced in this regime. This reduction also leads to numerical difficulties in measuring the coherence quality (Fig. 15a).

To test for a systematic relation between the degree on nonlinearity and the peakedness of the spectral coherence, we introduce a simple measure of "effective nonlinearity" in the next section.

3.4.2 Resonance in information transfer increases with degree of nonlinearity

A practical feature of the static nonlinearity model is that—depending on the nonlinearity's "location" relative to the distribution of membrane voltages that are passed through it and depending on its steepness—the degree of nonlinearity the membrane voltages are subjected to can be varied systematically. For example, if F is shallow (small slope) there is a broad range of voltage values around the inversion point of F that will be transformed in an essentially linear way. For narrow distributions of voltages around the inversion point, the output of the system $F(V(t))$ suffers only a weak nonlinear distortion. In contrast, very broad distributions of voltage responses or very steep nonlinearities result in output values $F(V(t))$ that are substantially distorted.

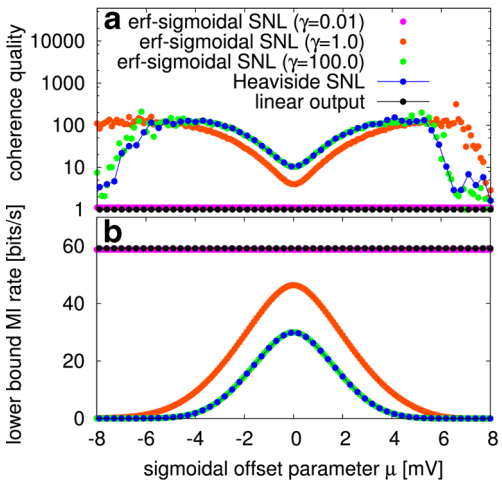

Fig. 15 The relative position between the static nonlinearity and the voltage distribution (i.e. the offset μ) affects coherence quality and mutual information rate. **a** Coherence quality as a function of μ (erf nonlinearity) for three different slope parameters $\gamma \in \{0.01, 1, 100\}$ and the Heaviside static nonlinearity; resonator cartoon linear subthreshold dynamics. **b** Lower bound mutual information rate (MI) as a function of μ

For a given distribution of the linear voltage responses, variation of either offset or slope factor of the nonlinearity changes the effective nonlinearity that the output $F(V)$ of the system was subjected to. A simple measure of this "effective nonlinearity", Γ is based on the distribution of the values of the local slopes $F'(V)$ of the static nonlinearity weighted by the distribution of linear voltages V subjected to it. The higher the values Γ, the more nonlinear the input-output transformation (for details see Section 2.2).

Figure 16 reveals a the systematic relation between the "effective nonlinearity" and the peakedness of the spectral coherence. The more nonlinear the input-output transformation, the higher the quality value of the coherence (Fig. 16a). In contrast, the more nonlinear the system, the lower the mutual information rate (Fig. 16b). In agreement with the results of the other models studied here, the emergence of a band-pass filter on information is accompanied by a reduction of the total information rate (see Fig. 16b). Note that the application of a static nonlinearity allows an analytical approach based on results developed by Bussgang (1952) resulting in expressions for all relevant spectral characteristics including the coherence function. For the sake of readability the corresponding formulas are not included.

To conclude, we can establish a positive correlation between the "effective nonlinearity" of the static transformation and the emergence of a band-pass filter on informa-

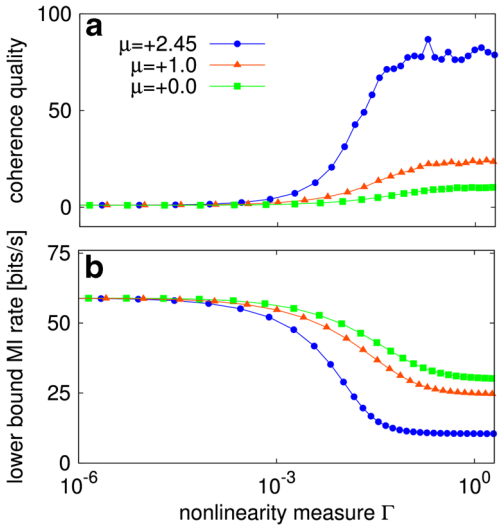

Fig. 16 Information rate and quality factor of the coherence crucially depend on properties of the nonlinearity. Coherence quality monotonically increases with the effective nonlinearity Γ (**a**), while the mutual information rate (lower bound) decreases (**b**). Note that the effective nonlinearity Γ depends on the slope factor γ of the static nonlinearity (see also Fig. 3 in Section 2), which was varied here. For each curve, the offset μ was fixed (see legend), but γ—and consequently the effective nonlinearity—was varied. Linear dynamics with parameters of the resonator cartoon

tion. Highly nonlinear input-output transformations lead to a band-pass filter on information with reduced information rate, whereas an almost linear transformation results in a broadband filter with high information rate.

4 Summary and conclusions

In resonant neurons, the impedance function of the subthreshold membrane potential is peaked, reflecting the fact that membrane-potential responses to input signals in this preferred frequency range are largest in amplitude. Such properties can arise from simple linear dynamics, such as those captured by the subthreshold part of resonate-and-fire neuron models. It is less well acknowledged, however, that the coherence function for such a linear system does not exhibit a resonance, i.e. acts as low-pass filter on information in the subthreshold membrane potential, despite the resonance in voltage amplitudes. Does this mean that resonant neuronal properties are irrelevant for the frequency preference of information transfer? In this study, we show that, indeed, resonant properties at the level of subthreshold voltage amplitudes can be imprinted onto the information transfer at the level of spikes when nonlinearities come into play. A spike threshold, in particular, is instrumental for subthreshold resonances to shape preferred frequency bands of information transfer by spikes.

Three types of nonlinearities, two of which generate spiking responses, were considered in this study: (1) a fixed voltage threshold in a resonate-and-fire model, (2) a nonlinear, conductance-based model, as well as (3) a simple static nonlinearity acting directly on the subthreshold membrane voltage. In all three models, the coherence function of the model output showed a resonant peak close to the frequency of the subthreshold membrane resonance. Interestingly, spiking is not necessarily required, as illustrated for the system with static nonlinearity. Here, no spikes are generated, but the linear voltage response is passed through a static nonlinear function. This system also underlines that the degree of nonlinearity (here estimated by the "effective nonlinearity") and the peakedness of the spectral coherence function are positively correlated.

Information filtering has been the subject of a number of theoretical and experimental studies. The standard one-dimensional integrate-and-fire model consistently displays low-pass filtering (Stein et al. 1972; Vilela and Lindner 2009; Lindner 2014) in the sense that the coherence displays a global maximum at zero frequency, hence, the standard IF model transmits most information in a low-frequency band. Remarkably, this numerical finding seems to hold true irrespective of the specific subthreshold dependence on the voltage (so far studied for the perfect, leaky, and quadratic integrate-and-fire models) and remains unaffected by the choice of the firing regime (pacemaker-like regular firing, Poisson-like firing, or bursting spike activity). In contrast to this, experimentally, coherence functions (or the corresponding lower-bound mutual-information-rate density) attaining a global maximum at *non-vanishing* frequency have been observed, e.g. in vestibular (Sadeghi et al. 2007) and auditory afferents (Rieke et al. 1995), in the visual system (Warland et al. 1997) and the electro-sensory system (Chacron et al. 2003). These results raise the question which features of the neural dynamics could be responsible for such a shaping of the coherence function, in particular, for a suppression of the information transmission at low frequencies.

Previous work has demonstrated that mechanisms at the population level or based on synaptic dynamics can cause a shift of the optimal frequency band of information transmission to higher frequencies. In Droste et al. (2013) it has been theoretically shown that heterogeneous synaptic plasticity can lead to pronounced low-pass or high-pass filtering of information for signals that arrive through facilitating and depressing synapses, respectively; a condition for this effect is the presence of at least two distinct signals as is observed, for instance, in the case of multi-sensory integration (Stein and Stanford 2008). At the neural population level, spikes that are fired in synchrony by two or more cells, preferentially encode information about higher frequency bands of a common stimulus signal - a finding that has been made experimentally for electro-sensory afferents in weakly electric fish (Middleton et al. 2009) and could be theoretically explained by the shaping of noise power in the synchrony code (Sharafi et al. 2013).

Our paper adds another possible mechanism of information band-pass filtering, based on the multidimensional subthreshold voltage dynamics seen in many neurons and, in particular, in resonant cells. In contrast to the above, this mechanism originates in the *cellular dynamics of a single cell* and should be experimentally well distinguishable from the other possible causes. Our simulation results suggest that a single neuron with a pronounced subthreshold resonance may function as a band-pass filter of information with respect to a current stimulus. This filter effect will be especially effective if the neuron is kept in an irregular firing regime with high CV, which is, remarkably, the kind of spike statistics that is typical for cortical cells. This finding is in line with previous results of Richardson et al. (2003) who found that the subthreshold frequency preference is reflected in the suprathreshold firing regime at the level of firing rate responses. However, it is surprising that this holds true at the level of information filtering, described by the coherence function Eq. (28), which also takes into account the spike-train-power spectrum and not just the squared cross spectrum.

Frequency selectivity is relevant for sensory peripheries, where information transfer between external stimulus and neuronal response directly reflects the obvious neuronal function of capturing relevant information from the environment. Specifically, if behaviorally relevant stimuli are rhythmic, resonant filter properties at the level of amplitudes and information may contribute to an efficient processing of signals. Such systems include many insect auditory systems, whose calling- and courtship songs exhibit a pronounced and species-specific rhythmicity (see, for example, Webb et al. 2007; Rau et al. 2015).

Nevertheless, this study also demonstrates that interpretations need to be tied to neuronal function: while the selectivity of frequency tuning on the level of information transmission can be increased through a combination of subthreshold resonance and (spiking) nonlinearities, overall information transmission (across all frequency bands) is inversely related. We showed that the increase in frequency preference of information transfer (i.e. a larger quality factor of the spectral coherence) comes at the cost of a reduction in the information transfer at other, predominantly lower, frequencies. From an evolutionary perspective, sensory systems may hence be ill advised to rely on resonances too early in their sensory periphery if the frequency content of relevant signals is broad. The stronger the peakedness in the coherence, the more specialized is the system (and the lower is the amount of information captured in other frequency regions). From the point of view of information transfer in such systems either low-pass subthreshold dynamics of single neurons or very weak nonlinearities (including forms of graded transmission) may prevail.

In summary, our study shows that wherever rhythmic signals play an important role—in mammalian systems, for example, reflected at the macroscopic level of the EEG, local field potential oscillations, as well as subthreshold oscillations of the membrane potential (Hutcheon and Yarom 2000; Buzsáki and Draguhn 2004)—nonlinearities in combination with subthreshold resonance can contribute to a frequency specific information transfer. Our study hence contributes to a better understanding of how cell-intrinsic properties shape the information that is available to downstream neurons via spikes. In general, linear systems driven with broadband noise do not exhibit resonances in the coherence (see Eq. (30)). Hence, our insights may also bear relevance for other biological systems, such as metabolic and signaling cascades, that exhibit substantial nonlinearities.

Acknowledgments This work was supported by grants from the BMBF (01GQ0901,01GQ0972,01GQ1001A,01GQ1403) and Deutsche Forschungsgemeinschaft (SFB 618(B1)).

Conflict of interests The authors declare that they have no conflict of interest.

Appendix A

A.1 Gradual transitions from resonators to integrators

Here, we present our numerical scheme to differentiate gradually between resonators and integrators. This allows us to study the relationship between the power filter properties and the information filter properties of these neuron models. The question arises whether there is a relation between impedance and coherence quality. Therefore we have to vary the impedance quality with respect to certain constraints. These constraints are experimentally motivated and should hold under variation of the impedance quality

a) resonance frequency is fixed (5 Hz, 9.5 Hz, 15 Hz),
b) natural frequency is smaller than resonance frequency (see Fig. 10 in Erchova et al. 2004), here: $\frac{f_{nat}}{f_{\mathrm{res}}} \approx 0.8$,
c) band-with of the impedance resonance should be proportional to the resonance freq. (see Fig. 7B in Erchova et al. 2004)
d) impedance quality should be varied in a systematic way,

We implemented a numerical scheme which solves a problem under these constraints. It turned out that the resistance of the inductor R_{L} is a suitable parameter to vary the impedance quality with the above described constraints. Suitable means that the experimentally observed parameter set of the stellate cell should lie on our parameterization manifold (see Fig. 17).

Figure 17a–b shows how the increase of the resistance R_{L} increases monotonically the impedance quality Q_Z and changes the damping factor ζ, the membrane resistance R, and the inductance L.

We display in Fig. 17e the expected relationship between the damping factor ζ and the impedance quality: with increasing damping factor the impedance quality decreases. These approximately 75.000 parameter sets are then used to simulate the resonate-and-fire neuron model within different excitable regimes (variation of DC input I_0 at fixed $D, D_{\mathrm{OU}}, V_{reset}, \tau_{\mathrm{abs}}$) at different impedance resonance frequencies (see Figs. 9–11) in order to reveal the dependence of the filtering properties between power filtering, described by the impedance function and information filtering, described by the coherence function.

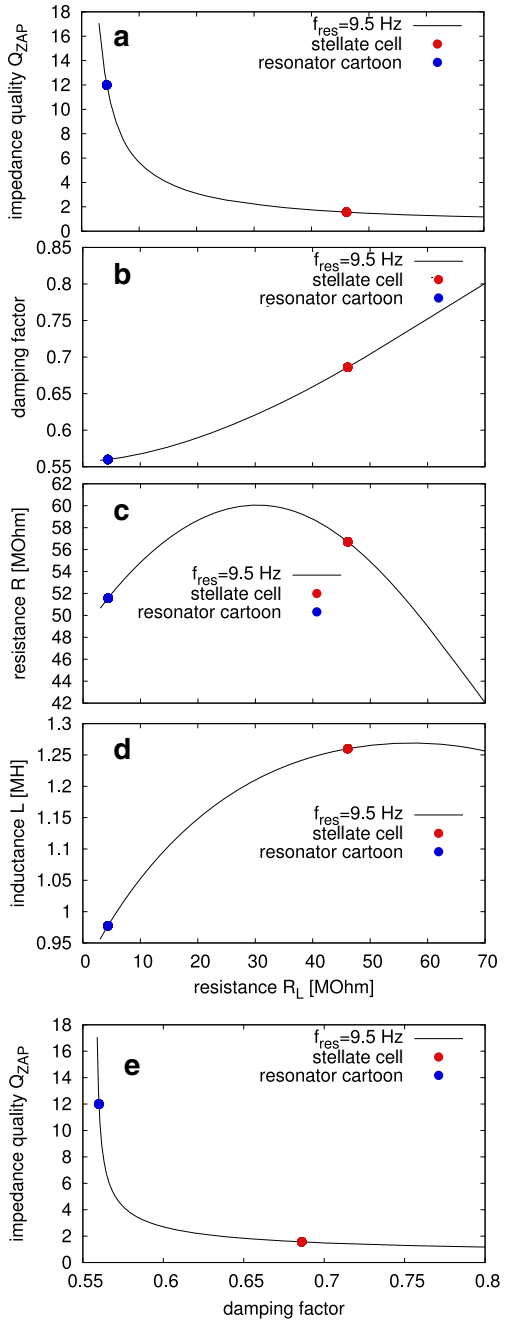

Fig. 17 Parameter sets yielding the same resonance frequency of the impedance in the linear, subthreshold dynamics. **a** Variation of impedance quality. By fixing the resonance frequency and changing the resistance of the inductor R_L one can systematically vary the impedance quality. This way gradual transitions from resonators to integrators (including the physiological parameter set of the stellate cell, red data point) were obtained. **b–d** Lines of equal resonance frequency in subspaces of parameters of the subthreshold dynamics of the RF model (resistance R_L versus damping factor, resistance R, and inductance L, respectively). **e** Impedance quality decreases with an increasing damping factor

References

Alonso, A., & Llinas, R.R. (1989). Subthreshold Na^+-dependent theta-like rhythmicity in stellate cells of entorhinal cortex layer-II. *Nature*, *342*, 175.

Badel, L., Lefort, S., Brette, R., Petersen, C.C.H., Gerstner, W., & Richardson, M.J.E. (2008). Dynamic I-V curves are reliable predictors of naturalistic pyramidal-neuron voltage traces. *Journal of Neurophysiology*, *99*, 656.

Borst, A., & Theunissen, F. (1999). Information theory and neural coding. *Nature Neuroscience*, *2*, 947.

Brunel, N., Hakim, V., & Richardson, M.J.E. (2003). Firing-rate resonance in a generalized integrate-and-fire neuron with subthreshold resonance. *Phys Rev E*, *67*, 051,916.

Bussgang, J.J. (1952). Crosscorrelation functions of amplitude-distorted Gaussian signals. *Research Lab. Electron*.

Buzsáki, G., & Draguhn, A. (2004). Neuronal oscillations in cortical networks. *Science*, *304*(5679), 1926–1929.

Chacron, M.J., Doiron, B., Maler, L., Longtin, A., & Bastian, J. (2003). Non-classical receptive field mediates switch in a sensory neuron's frequency tuning. *Nature*, *423*, 77.

Droste, F., Schwalger, T., & Lindner, B. (2013). Interplay of two signals in a neuron with short-term synaptic plasticity. *Frontiers in Computational Neuroscience*, *7*, 86.

Engel, T.A., Schimansky-Geier, L., Herz, A.V.M., Schreiber, S., & Erchova, I. (2008). Subthreshold membrane-potential resonances shape spike-train patterns in the entorhinal cortex. *Journal of Neurophysiology*, *100*, 1576.

Erchova, I., Kreck, G., Heinemann, U., & Herz, A. (2004). Dynamics of rat entorhinal cortex layer II and III cells: characteristics of membrane potential resonance at rest predict oscillation properties near threshold. *Journal of Neurophysiology*, *560*(Pt 1), 89.

Frigo, M., & Johnson, S.G. (2005). The design and implementation of FFTW3. *Proceedings of the IEEE*, *93*(2), 216–231.

Gabbiani, F. (1996). Coding of time-varying signals in spike trains of linear and half-wave rectifying neurons. *Network-Comp Neural*, *7*, 61.

Galassi, M., Davies, J., Theiler, J., Gough, B., Jungman, G., Alken, P., Booth, M., & Rossi, F. (2009). GNU scientific library reference manual-(v1. 12). Network Theory Ltd.

Gimbarzevsky, B., Miura, R.M., & Puil, E. (1984). Impedance profiles of peripheral and central neurons. *Canadian Journal of Physiology and Pharmacology*, *62*(4), 460–462.

Gloveli, T., Schmitz, D., Empson, R.M., & Heinemann, U. (1997). Frequency-dependent information flow from the entorhinal cortex to the hippocampus. *Journal of Neurophysiology*, *78*(6), 3444–3449.

Gutfreund, Y., Segev, I., et al. (1995). Subthreshold oscillations and resonant frequency in guinea-pig cortical neurons: physiology and modelling. *Journal of Neurophysiology*, *483*(Pt 3), 621–640.

Gutkin, B.S., & Ermentrout, G.B. (1998). Dynamics of membrane excitability determine interspike interval variability: a link between spike generation mechanisms and cortical spike train statistics. *Neural Computation*, *10*, 1047.

Hu, H., Vervaeke, K., & Storm, J.F. (2002). Two forms of electrical resonance at theta frequencies, generated by M-current, h-current and persistent Na^+ current in rat hippocampal pyramidal cells. *The Journal of Physiology*, *545*(3), 783–805.

Hutcheon, B., & Yarom, Y. (2000). Resonance, oscillation and the intrinsic frequency preferences of neurons. *Trends in Neurosciences*, *23*(5), 216–222.

Hutcheon, B., Miura, R.M., & Puil, E. (1996). Models of subthreshold membrane resonance in neocortical neurons. *Journal of Neurophysiology*, *76*(2), 698–714.

Izhikevich, E.M. (2001). Resonate-and-fire neurons. *Neural Networks*, *14*, 883.

Izhikevich, E.M. (2007). *Dynamical systems in neuroscience: the geometry of excitability and bursting*. Cambridge: The MIT Press.

Kloeden, P., & Platen, E. (1992). *Numerical Solution of Stochastic Differential Equations*. Berlin: Springer.

Lindner, B. (2014). Low-pass filtering of information in the leaky integrate-and-fire neuron driven by white noise. In *International Conference on Theory and Application in Nonlinear Dynamics (ICAND 2012)* (pp. 249–258). Berlin: Springer.

Lindner, B., Schimansky-Geier, L., & Longtin, A. (2002). Maximizing spike train coherence or incoherence in the leaky integrate-and-fire model. *Phys Rev E*, *66*, 031,916.

Lindner, B., García-Ojalvo, J., Neiman, A., & Schimansky-Geier, L. (2004). Effects of noise in excitable systems. *Physics Reports*, *392*, 321.

Lindner, B., Gangloff, D., Longtin, A., & Lewis, J.E. (2009). Broadband coding with dynamic synapses. *The Journal of Neuroscience*, *29*, 2076.

Mauro, A., Conti, F., Dodge, F., & Schor, R. (1970). Subthreshold behavior and phenomenological impedance of the squid giant axon. *The Journal of General Physiology*, *55*(4), 497–523.

Middleton, J.W., Longtin, A., Benda, J., & Maler, L. (2009). Postsynaptic receptive field size and spike threshold determine encoding of high-frequency information via sensitivity to synchronous presynaptic activity. *Journal of Neurophysiology*, *101*, 1160.

Morris, C., & Lecar, H. (1981). Voltage oscillations in the barnacle giant muscle fiber. *Biophysical Journal*, *35*, 193.

Puil, E., Meiri, H., & Yarom, Y. (1994). Resonant behavior and frequency preferences of thalamic neurons. *Journal of Neurophysiology*, *71*(2), 575–582.

Rau, F., Clemens, J., Naumov, V., Hennig, R.M., & Schreiber, S. (2015). Firing-rate resonances in the peripheral auditory system of the cricket, gryllus bimaculatus. *Journal of Neurophysiology*. submitted.

Rice, S.O. (1944). Mathematical analysis of random noise. *Bell Syst Tech J*, *23*, 282.

Richardson, M.J.E., Brunel, N., & Hakim, V. (2003). From subthreshold to firing-rate resonance. *Journal of Neurophysiology*, *89*, 2538.

Rieke, F., Bodnar, D., & Bialek, W. (1995). Naturalistic stimuli increase the rate and efficiency of information transmission by primary auditory afferents. *Proceedings of the Biological Sciences*, *262*, 259.

Rieke, F., Warland, D., de Ruyter van Steveninck, R., & Bialek, W. (1996). *Spikes: Exploring the neural code*. Cambridge: MIT Press.

Rinzel, J., & Ermentrout, G.B. (1989). Analysis of neural excitability and oscillations. In *Methods in Neuronal Modeling* (pp. 135–169). Cambridge: MIT Press.

Risken, H. (1984). *The Fokker-Planck equation*. Berlin: Springer.

Roddey, J.C., Girish, B., & Miller, J.P. (2000). Assessing the performance of neural encoding models in the presence of noise. *Journal of Computational Neuroscience*, *8*(2), 95–112.

Rosenbaum, R., Rubin, J., & Doiron, B. (2012). Short term synaptic depression imposes a frequency dependent filter on synaptic information transfer. *PLoS Computational Biology*, *8*, e1002, 557.

Rotstein, H.G., & Nadim, F. (2014). Frequency preference in two-dimensional neural models: a linear analysis of the interaction between resonant and amplifying currents. *Journal of Computational Neuroscience*, *37*(1), 9–28.

Sadeghi, S.G., Chacron, M.J., Taylor, M.C., & Cullen, K.E. (2007). Neural variability, detection thresholds, and information transmission in the vestibular system. *The Journal of Neuroscience*, *27*(4), 771.

Schreiber, S. (2004). *Frequency preference and reliability of signal integration: the role of intrinsic conductances. PhD thesis*. Berlin: Humboldt University.

Schreiber, S., Erchova, I., Heinemann, U., & Herz, A.V. (2004). Subthreshold resonance explains the frequency-dependent integration of periodic as well as random stimuli in the entorhinal cortex. *Journal of Neurophysiology*, *92*(1), 408–415.

Sharafi, N., Benda, J., & Lindner, B. (2013). Information filtering by synchronous spikes in a neural population. *Journal of Computational Neuroscience*, *34*, 285.

Stein, B.E., & Stanford, T.R. (2008). Multisensory integration: current issues from the perspective of the single neuron. *Nature Reviews Neuroscience*, *9*, 255.

Stein, R.B., Holden, A.V., & French, A.S. (1972). Frequency-response, coherence, and information capacity of 2 neuronal models. *Biophysical Journal*, *12*, 295.

Vilela, R.D., & Lindner, B. (2009). A comparative study of three different integrate-and-fire neurons: spontaneous activity, dynamical response, and stimulus-induced correlation. *Physical Review E*, *80*, 031,909.

Warland, D.K., Reinagel, P., & Meister, M. (1997). Decoding visual information from a population of retinal ganglion cells. *Journal of Neurophysiology*, *78*, 2336.

Webb, B., Wessnitzer, J., Bush, S., Schul, J., Buchli, J., & Ijspeert, A. (2007). Resonant neurons and bushcricket behaviour. *Journal of Comparative Physiology. A*, *193*(2), 285–288.